The Aeronautical Journal (2023), **127**, pp. 139–162
doi:10.1017/aer.2022.47

REGULAR PAPER

Finite-time velocity-free trajectory tracking control for a stratospheric airship with preassigned accuracy

Y. Wu, Q. Wang* and D. Duan

School of Aeronautics and Astronautics Shanghai Jiao Tong University Shanghai PR China
*Corresponding author. Email: quanbaowang@sjtu.edu.cn

Received: 28 September 2021; **Revised:** 30 March 2022; **Accepted:** 11 April 2022

Keywords: Stratospheric airship; Underactuation; Output feedback; Finite-time control; Preassigned accuracy

Abstract
This paper concentrates on the trajectory tracking problem for a stratospheric airship subject to underactuated dynamics, unmeasured velocities, modeling inaccuracies and environmental disturbances. First, a coordinate transformation is performed to solve the underactuated issue, which simultaneously permits a priori assignment of the tracking accuracy. Second, a finite-time observer is integrated into the control structure to offer the exact information of unmeasured velocities and uncertainties in an integral manner. Then, by combining the backstepping technique with the method of adding a power integrator, a new output-feedback control strategy is derived with several salient contributions: (1) the airship's position errors fall into a predetermined residual region near zero within a finite settling time and stay there, while all the closed-loop signals maintain bounded during operation; and (2) no artificial neural networks and filters are adopted, resulting in a low-complexity control property. Furthermore, the presented method can be extended readily to a broad range of second-order mechanical systems as its design builds upon a transformed system model. Rigorous mathematical analysis and simulations demonstrate the above theoretical findings.

Nomenclature

NN	neural network
LOS	line of sight
API	adding a power integrator
FTO	finite-time observer
ERF	earth reference frame
BRF	body-fixed reference frame
CV	centre of volume
AUV	autonomous underwater vehicle
EL	Euler–Lagrange
CFB	command-filter backstepping
IAE	integrated absolute error
ITAE	integrated time absolute error
MIAC	mean integrated absolute control
$\mathbb{R}_{>0}$	set of positive real numbers
I_n	identity matrix of size n
$\mathbb{R}^n$	n-dimensional Euclidean space
$o_g x_g y_g z_g$	earth reference frame (ERF)
$o x_b y_b z_b$	body-fixed reference frame (BRF)
$[x,\ y]$	positions of the CV in ERF
ψ	yaw attitude in BRF
$[u,\ v,\ r]$	velocities in BRF

m_i	mass, $i = u, v, r$
d_i	damping term, $i = u, v, r$
τ_i	control input, $i = u, r$
δ_i	system uncertainties and external disturbances, $i = u, v, r$
δ_i'	cross-coupling term, $i = u, v, r$
m_i'	uncertain part of $m_i, i = u, v, r$
d_i'	uncertain part of $d_i, i = u, v, r$
δ_{dis_i}	wind resistance, $i = u, v, r$
$[x_d,\ y_d]$	reference trajectory

1.0 Introduction

Recently, the stratosphere has received considerable attention from the modern aviation and aerospace industry that endeavors to exploit its stable atmospheric conditions [1–3]. This dramatically accelerates the development of the long-dwell stratospheric airship [4], which is a typical lighter-than-air aircraft that plays various roles from telecommunication to space-like observation outpost, similar to satellites [5–8]. To accomplish diverse mission objectives, driving the airship to reach and follow a time parameterised reference route, also termed as trajectory tracking control, is the most fundamental flight control task [9–11]. However, high nonlinearities, strong couplings, modeling inaccuracies, and unpredictable disturbances render the trajectory tracking control design quite intractable.

To date, many powerful control methodologies have been applied to solve this problem, such as adaptive control [12], backstepping method [9, 13], and sliding mode control [14]. Taking several kinds of uncertainty into consideration, Xiao et al. [14] proposed an adaptive integral sliding mode controller for an airship. However, no effective modification technique was provided to eliminate control chattering, thus yielding its implementation impossible. In other works [6, 10, 15–17], the unmodeled dynamics and external disturbances were identified and compensated by neural networks (NNs) or fuzzy logic systems (FLSs). However, the employment of NNs and FLSs will inevitably make the controller computationally expensive due to their inherent attributes. Furthermore, it should be emphasised that these controllers only apply to fully actuated airships, which, in general, cannot guarantee the tracking behaviour of underactuated ones.

In reality, most of the potential application scenarios of stratospheric airships are always associated with horizontal motion, and the stratospheric airship can automatically maintain the cruise altitude via an independent lift adjustment system alone [3, 15, 17, 18]. Given this fact, this work focuses on the horizontal trajectory tracking design for one kind of airship. At present, several challenging issues concerning this subject are still open, three of which are discussed in this paper. The first one is the underactuated problem. The conventional teardrop-shaped airship, operating at a proper flight altitude, is a typically underactuated system [6, 17], primarily due to the non-existence of an independent actuator producing the lateral force to command the sway dynamics. This poses new challenges as the lateral underactuation imposes a non-integrable restriction on the acceleration of the airship, and therefore it has become an important topic of research [3, 19–22]. Toward underactuated airships and other types of underactuated vehicles, several controllers have been proposed, both of which have great reference values for us, including the waypoint navigation method [23], the transverse function control [20], and the line of sight (LOS) approach [6, 10, 17, 21]. The controller grounded on the waypoint navigation method [23] demands pre-planning an optimal course that aligns with the direction of the wind, which may be suitable for hovering control rather than trajectory tracking control. The transverse function control also needs dynamic extension [20] to accommodate the lateral underactuation, which admittedly complicates the plant model. Although the LOS approach is deemed an efficient guidance law for underactuated vehicles, LOS-based trajectory tracking controllers require confining the tracking error of yaw angle ψ_e to the interval $\left(-\frac{\pi}{2}, \frac{\pi}{2}\right)$ for $\forall t \geq 0$. Generally, the error-constrained problem is unavoidably linked to rather complex nonlinear mappings. Some prime examples can be found in the works of Jia et al. [21] and Wu et al. [10], both of which introduced barrier functions and error-dependent transformations to meet such a restrictive condition.

https://doi.org/10.1017/aer.2022.47 Published online by Cambridge University Press

The second issue is about the performance specification. Note that some previous designs [6, 9, 14, 15, 18, 23] can only ensure the equilibrium point of error dynamics is of asymptotic stability, namely, that the settling time, a critical indicator in control design for airships, is infinity. To this end, the finite-time stability and stabilisation theory was established [12, 24–26], permitting a bounded convergence time. Until now, the finite-time control has been an active research area because of its good control qualities, such as the faster decay rate, higher tracking accuracy, and better disturbance rejection property, and has been rapidly applied in various fields, including strict-feedback or nonstrict-feedback nonlinear systems [16, 27, 28], uncertain manipulators [29], and rigid spacecrafts [30, 31]. Nevertheless, own to the coupled nonlinearities in the kinematic equation of airships, extending these finite-time controllers to the trajectory tracking control design for airships is nontrivial, especially for underactuated ones. For fully actuated airships, several finite-time trajectory tracking or path following control algorithms were constructed [10, 17], where the hard computation of time derivatives of virtual control laws was obviated through filter tools. Though the filter can avoid repeated differentiation, it still structurally increases the complexity of control systems. Attributed to the adding a power integrator (API) method, a range of finite-time control strategies were formulated for airships and other mechanical systems without filters [30–35]. It should be noted that the power terms used in these API-based methods are strictly constrained to be an even integer or a ratio of two odd integers. Furthermore, in the above finite-time controllers, the prior designation of the size of the residual set is infeasible in that the steady-state accuracy counts on some unknowable model parameters and uncertainty bounds.

The third issue is related to the output feedback. Careful reviews of the above results reveal that most entail full state measurement. However, such a demand is hardly guaranteed in some practical applications. For example, the velocity information of airships cannot always be available at each instant coming from considerations of sensor faults. Inspired by this observation, some notable works used high-gain observers [21], sliding model observers [10], and fuzzy observers [27] to achieve output-feedback control. Although the maturity of the current output-feedback control, the finite-time trajectory tracking control design for airships subject to underactuated dynamics, unmeasured velocities, modeling imprecisions, and external disturbances is still a challenging control problem that needs more in-depth research.

Motivated by the above discussion, this paper proposes a novel approach by a combined application of the backstepping method, the API technique, and the idea of coordinate transformation. Our contributions are as follows:

1. Compared to the asymptotic control algorithms [6, 9, 14, 15, 18, 23], our approach allows tracking behaviour to be preassigned by the operator, i.e. it drives the position errors of the airship into a preset range near zero within a finite settling time.
2. By employing some useful lemmas, we relax the strong constraints placed on the power terms [30–35], broadening the set of possible design parameters. Moreover, unlike the sliding mode controllers [11, 14, 15], our control signal is continuous and chattering-free.
3. A coordinate transformation is performed herein. Consequently, this work forsakes the extra dynamics needed in the transverse function control [20], and lifts the restriction of LOS-based controllers [10, 21]. Furthermore, the presented controller can be extended easily to a wide range of second-order mechanical systems as its design counts on a transformed equivalent model.
4. Our method is structurally less demanding; no tools for filtering [6, 9, 14, 15, 18, 23] are involved, and no arduous computation of analytic differentiation required in the backstepping technique [20] is performed. Furthermore, this work realises velocity-free control and is robust enough in that it establishes a finite-time observer (FTO) to reconstruct unmeasured velocities and unpredictable uncertainties in a integral manner. In contrast to NN or FLS approximation [6, 10, 15–17, 27], the FTO can sharply lighten the calculational burden, making it particularly appealing for control applications.

https://doi.org/10.1017/aer.2022.47 Published online by Cambridge University Press

Section 2 presents the preliminaries and control objective. Section 3 elucidates the coordinate conversion to cope with lateral underactuation. The major control design procedure and Lyapunov analysis are given in Section 4. Section 5 delineates the simulation results. Section 6 concludes this brief.

2.0 Preliminaries and problem formulation

2.1 Preliminaries

The notation $\mathbb{R}_{>0}$ is referred to the set of positive real numbers, and the notation $I_n \in \mathbb{R}^{n\times n}$ represents the unit matrix. $|\cdot|$ is the absolute value of a scalar, while $\|\cdot\|$ is the Euclidean 2-norm of a vector or the induced 2-norm of a matrix. Given $\iota > 0$ and $\ell = [\ell_1, \ell_2, \ldots, \ell_n]^T \in \mathbb{R}^n$, $|\ell|$, $|\ell|^\iota$, and $\lfloor \ell \rceil$ refer to $|\ell| = [|\ell_1|, |\ell_2|, \ldots, |\ell_n|]^T$, $|\ell|^\iota = [|\ell_1|^\iota, |\ell_2|^\iota, \ldots, |\ell_n|^\iota]^T$, and $\lfloor \ell \rceil = diag\,\{\ell_1, \ell_2, \ldots, \ell_n\}$, respectively. Denote $sig^\iota(\ell) = \left[sig^\iota(\ell_1), sig^\iota(\ell_2), \ldots, \; sig^\iota(\ell_n)\right]^T$, where $sig^\iota(\ell_i) = |\ell_i|^\iota sgn(\ell_i)$ $(i = 1, \ldots, n)$, and $sgn(\cdot)$ is the standard signum function given by

$$sgn(x) = \begin{cases} -1, & if \;\; x < 0 \\ 0, & if \;\; x = 0. \\ 1, & if \;\; x > 0 \end{cases} \tag{1}$$

At this stage, we provide some useful definitions and lemmas used later.

Consider the dynamical system

$$\dot{x} = f(x(t)), x(0) = x_0, \;\; f(0) = 0, x \in \mathbb{U}_0 \subset \mathbb{R}^n, \tag{2}$$

where x is a state vector, the time variable t varies from 0 to ∞, $\mathbb{U}_0$ is a finite open set containing the origin $x = 0$, and $f(\cdot) : \mathbb{R}^n \to \mathbb{R}^n$, well-defined on $\mathbb{U}_0$, is a continuous differentiable nonlinear vector function.

Definition 1 (see the work of Sun et al. [16]). *If the equilibrium point $x = 0$ of system (2) is referred to as a (locally) asymptotic stable node and for any initial state $x_0 \in \mathbb{U}_0$, there exist $\varepsilon \in \mathbb{R}_{>0}$ and a settling time function $T(\varepsilon, x_0) < \infty$ such that $\|x(t)\| \le \varepsilon, \forall t > T(\varepsilon, x_0)$, then it is true that system (2) has a (locally) finite-time stable equilibrium point at $x = 0$. Furthermore, if $\mathbb{U}_0 = \mathbb{R}^n$, then $x = 0$ is globally finite-time stable.*

Lemma 1 (see the work of Sun et al. [16]). *Suppose there exists a Lyapunov function $V(x)$ defined in domain $\mathbb{U}_0$, and the time derivative of $V(x)$ along the trajectory of system (2) satisfies*

$$\dot{V}(x) \le -qV^g(x) + p, \tag{3}$$

where $\{q, p\} \in \mathbb{R}_{>0}$, and $0 < g < 1$, then the system (2) is finite-time stable.

Lemma 2 (see the work of Sun et al. [16]). *For any $\{x, y\} \in \mathbb{R}$, the following inequality holds:*

$$|x|^m |y|^n \le \frac{m}{m+n} s |x|^{m+n} + \frac{n}{m+n} s^{-\frac{m}{n}} |y|^{m+n}, \tag{4}$$

where $\{m, n, s\} \in \mathbb{R}_{>0}$,

Lemma 3 (see the work of Zheng et al. [34]). *Let $\xi_i \in \mathbb{R}$, $i = 1, 2, \ldots, n$. Then*

$$\begin{aligned} &\left(\sum_{i=1}^n |\xi_i|\right)^\mu \le \sum_{i=1}^n |\xi_i|^\mu \le n^{1-\mu} \left(\sum_{i=1}^n |\xi_i|\right)^\mu \quad , \mu \in (0, 1]\,, \\ &\sum_{i=1}^n |\xi_i|^\mu \le \left(\sum_{i=1}^n |\xi_i|\right)^\mu \le n^{\mu-1} \sum_{i=1}^n |\xi_i|^\mu \quad , \mu \in (1, \infty)\,. \end{aligned} \tag{5}$$

https://doi.org/10.1017/aer.2022.47 Published online by Cambridge University Press

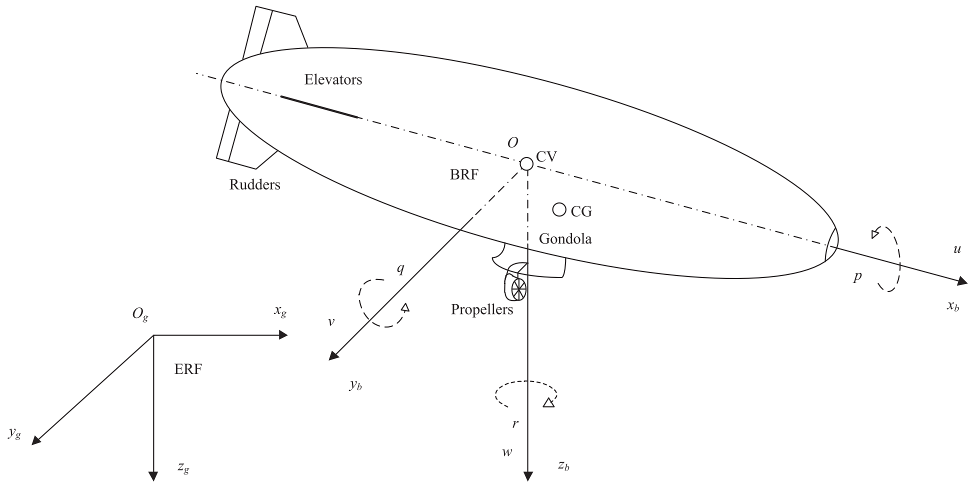

Figure 1. *Depiction of the stratospheric airship.*

Lemma 4 (see the work of Du et al. [30]). *If* $\vartheta_1 > 0$ *and* $0 < \vartheta_2 \leq 1$*, then*

$$|sig^{\vartheta_1\vartheta_2}(x) - sig^{\vartheta_1\vartheta_2}(y)| \leq 2^{1-\vartheta_2}|sig^{\vartheta_1}(x) - sig^{\vartheta_1}(y)|^{\vartheta_2}, \forall \{x, y\} \in \mathbb{R}. \tag{6}$$

Lemma 5 (see the work of Du et al. [30]). *For any* $\varsigma \in \mathbb{R}_+$ *and* $z \in \mathbb{R}$*, we have*

$$\frac{d}{dt}|z|^{\varsigma+1} = (\varsigma + 1)\, sig^{\varsigma}(z)\, \dot{z},\ \frac{d}{dt}sig^{\varsigma+1}(z) = (\varsigma + 1)\, |z|^{\varsigma}\dot{z}. \tag{7}$$

2.2 Airship model

Figure 1 displays the stratospheric airship with a typical streamline ballonet. The helium-filled ballonet generates an upward lift for the airship. The cargo bay fixed below the ballonet aims to house the onboard systems. The propulsive units mounted on both sides of the gondola furnish thrust for flight. The control surfaces (elevators and rudders) installed on the tail offer yawing and pitching moments.

To investigate the motion control of the airship, it is reasonable to establish the earth and body-fixed coordinate systems; see Fig. 1. The earth reference frame (ERF) has its origin o_g at a fixed point on the earth, the o_gx_g-axis points north, the o_gy_g-axis points east, and the o_gz_g-axis points to the earth's centre perpendicular to the plane $o_gx_gy_g$. The body-fixed reference frame (BRF) moving with the airship sets its origin o at the centre of volume (CV), the ox_b-axis points to the nose of the airship, the oy_b-axis points to the starboard side of the airship, and the oz_b-axis lying on the longitudinal axisymmetric plane of the airship normal to the plane ox_by_b.

Neglect the aeroelastic influences and regard the airship as a rigid body. Taken from the airship modeling technique [2, 9, 10, 14, 15, 17, 22, 23, 34], the airship model built around the horizontal motion can be directly given here, which is formulated by [6, 18, 36–38]

$$\begin{aligned}
\begin{bmatrix} \dot{x} \\ \dot{y} \\ \dot{\psi} \end{bmatrix} &= \begin{bmatrix} \cos(\psi) & -\sin(\psi) & 0 \\ \sin(\psi) & \cos(\psi) & 0 \\ 0 & 0 & 1 \end{bmatrix} \begin{bmatrix} u \\ v \\ r \end{bmatrix} = J(\psi)\, \nu, \\
\begin{bmatrix} m_u\dot{u} \\ m_v\dot{v} \\ m_r\dot{r} \end{bmatrix} &= \begin{bmatrix} m_v vr \\ -m_u ur \\ m_{uv} uv \end{bmatrix} - \begin{bmatrix} d_u u \\ d_v v \\ d_r r \end{bmatrix} + \begin{bmatrix} \tau_u \\ 0 \\ \tau_r \end{bmatrix} + \begin{bmatrix} \delta_u \\ \delta_v \\ \delta_r \end{bmatrix}.
\end{aligned} \tag{8}$$

https://doi.org/10.1017/aer.2022.47 Published online by Cambridge University Press

In the above equations, x, y are the CV's positions in the ERF, and ψ is the yaw attitude in the BRF; u, v, r are the surge velocity, lateral velocity and yaw angular velocity with respect to the BRF, respectively; m_i and d_i $(i = u, v, r)$ denote the mass and damping term [2, 19, 39], respectively; $m_{uv} = m_u - m_v$; $\tau = [\tau_u, \tau_r]^T$ is the actuating signal. $\delta = [\delta_u, \delta_v, \delta_r]^T$ characterises all the modeling imperfections and disturbances. To facilitate subsequent discussions, some of most fundamental assumptions are delineated below.

Assumption 1 (see other works [3, 10, 22]). *The airship is flying at a proper cruising altitude with stable meteorological conditions, while maintaining buoyancy-weight balance. The pitch and roll angle are very small such that the associated dynamics can be neglected.*

Assumption 2 (see other works [6, 19, 39]). *In this work, we suppose that δ_i $(i = u,v,r)$ takes the form*

$$\begin{cases} \delta_u = \delta'_u + m'_v vr - d'_u u - m'_u \dot{u} + \delta_{dis_u} \\ \delta_v = \delta'_v - m'_u ur - d'_v v - m'_v \dot{v} + \delta_{dis_v} \\ \delta_r = \delta'_r + m'_{uv} uv - d'_r r - m'_r \dot{r} + \delta_{dis_r} \end{cases}, \tag{9}$$

where δ'_i is the cross-coupling term, m'_i and d'_i are the uncertain part of m_i and d_i, respectively, and δ_{dis_i} characterises the slow time-varying wind resistance.

Remark 1. From Equation (8), the airship, operating in three degrees of freedom, only has two independent actuating signals (τ_u, τ_r) in surge and yaw, which poses a prominent obstacle to steering the airship alone through a scheduled trajectory with stringent time and performance requirements. Indeed, it is physically apparent that most surface vehicles (SVs) and autonomous underwater vehicles (AUVs) propelling themselves on a horizontal plane are underactuated, and the motion equations of SVs and AUVs are pretty similar to that of the underactuated airship [20, 21]. When designing the motion control algorithms for SVs and AUVs, the performance specifications, such as the convergent time and the residual set, always exist. Therefore, this work is constructive for motion control design for SVs and AUVs to some extent.

Remark 2. Some effective altitude control techniques [3, 10, 22], such as inflating and deflating valves, make Assumption 1 mild and realistic. Assumption 2 is frequently made in the works on horizontal motion control of airships [6, 19, 39]. It is also important to point out that the term δ'_i $(i = u, v, r)$ in Equation (9) is used to depict the coupling effects of pitch and roll.

2.3 Control objective

In this article, our control objective is to generate a control law for τ to be employed by the stratospheric airship in underactuated mode, such that, despite the adverse influences of unmeasured velocities and uncertainties, the position of the airship $\eta = [x, y]^T$ tracks with the scheduled route $\eta_d = [x_d, y_d]^T$ with a priori designate performance, i.e. such that the tracking error $e = \eta - \eta_d = [x_e, y_e]^T$ fulfills

$$\max\{|x_e|, |y_e|\} \le \epsilon, \forall t \ge T_f, \tag{10}$$

where ϵ represents the preassigned tracking accuracy, and $0 < T_f < \infty$ denotes the finite settling time. Meanwhile, all the closed-loop signals maintain bounded $\forall t \ge 0$.

Assumption 3. *The reference trajectory η_d and its derivatives up to $\ddot{\eta}_d$ are bounded, continuous, and available for $\forall t \ge 0$.*

https://doi.org/10.1017/aer.2022.47 Published online by Cambridge University Press

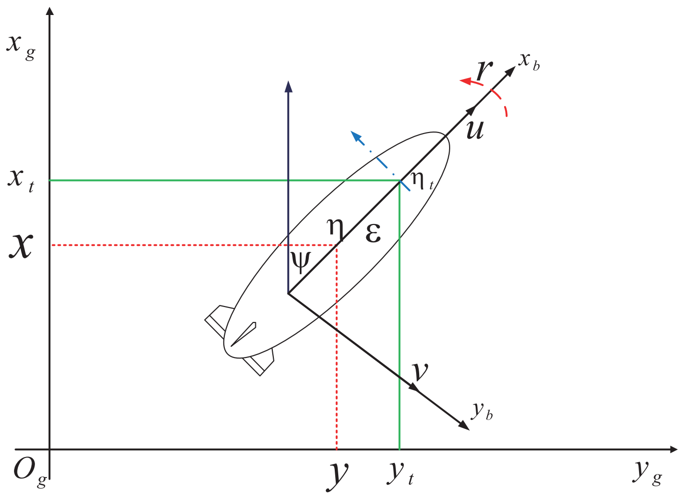

Figure 2. *Coordinate transformation.*

3.0 Coordinate transformation

To fix the underactuated issue, a coordinate transformation is first conducted, specified as

$$x_t = x + \epsilon \cos(\psi) \, , y_t = y + \epsilon \sin(\psi) \, , \tag{11}$$

where $\eta_t = \left[x_t, y_t\right]^T$ denotes a new position, and except for having the definition in Equation (10), ϵ also is the distance between η and η_d (see Fig. 2). Calculating the second-order time-derivative of η_t and taking Equation (8) into consideration yield

$$\begin{aligned} \ddot{x}_t &= \dot{u}\cos(\psi) - (\dot{v} + \epsilon\dot{r})\sin(\psi) - ur\sin(\psi) - \left(vr + \epsilon r^2\right)\cos(\psi) \, , \\ \ddot{y}_t &= \dot{u}\sin(\psi) + (\dot{v} + \epsilon\dot{r})\cos(\psi) + ur\cos(\psi) - \left(vr + \epsilon r^2\right)\sin(\psi) \, . \end{aligned} \tag{12}$$

Then, substituting Equation (8) for Equation (12), we obtain

$$\begin{aligned} \ddot{x}_t &= \frac{\cos(\psi)}{m_u}\tau_u - \frac{\epsilon\sin(\psi)}{m_r}\tau_r + F_x + \delta_{tfx}, \\ \ddot{y}_t &= \frac{\sin(\psi)}{m_u}\tau_u + \frac{\epsilon\cos(\psi)}{m_r}\tau_r + F_y + \delta_{tfy}, \end{aligned} \tag{13}$$

where

$$\begin{aligned} F_x = &\frac{m_v vr - d_u u}{m_u}\cos(\psi) + \frac{m_u ur + d_v v}{m_v}\sin(\psi) - \frac{m_{uv} uv - d_r r}{m_r}\epsilon\sin(\psi) \\ &- ur\sin(\psi) - \left(vr + \epsilon r^2\right)\cos(\psi) \, , \end{aligned} \tag{14}$$

$$\begin{aligned} F_y = &\frac{m_v vr - d_u u}{m_u}\sin(\psi) - \frac{m_u ur + d_v v}{m_v}\cos(\psi) + \frac{m_{uv} uv - d_r r}{m_r}\epsilon\cos(\psi) \\ &+ ur\cos(\psi) - \left(vr + \epsilon r^2\right)\sin(\psi) \, , \end{aligned} \tag{15}$$

$$\delta_{tfx} = \frac{\delta_u}{m_u}\cos(\psi) - \left(\frac{\delta_v}{m_v} + \frac{\epsilon\delta_r}{m_r}\right)\sin(\psi) \, , \tag{16}$$

$$\delta_{tfy} = \frac{\delta_u}{m_u}\sin(\psi) + \left(\frac{\delta_v}{m_v} + \frac{\epsilon\delta_r}{m_r}\right)\cos(\psi) \, . \tag{17}$$

https://doi.org/10.1017/aer.2022.47 Published online by Cambridge University Press

Denoting $\varkappa_1 = \eta_t$, $\varkappa_2 = \dot{\eta}_t$, $\digamma = \left[\digamma_x, \digamma_y\right]^T$, $\delta_{tf} = \left[\delta_{tfx}, \delta_{tfy}\right]^T$, and $\tau = [\tau_u, \tau_r]^T$, Equation (13) then can be rewritten in the synthetic form

$$\begin{aligned} \dot{\varkappa}_1 &= \varkappa_2, \\ \dot{\varkappa}_2 &= R(\psi)\, M_\epsilon \tau + \digamma + \delta_{tf}, \end{aligned} \tag{18}$$

where

$$R(\psi) = \begin{bmatrix} \cos(\psi) & -\sin(\psi) \\ \sin(\psi) & \cos(\psi) \end{bmatrix}, \quad M_\epsilon = \begin{bmatrix} \dfrac{1}{m_u} & 0 \\ 0 & \dfrac{\epsilon}{m_r} \end{bmatrix}. \tag{19}$$

Obviously, $R(\psi)\, R^T(\psi) = I_2$, and M_ϵ is a positive-definite diagonal matrix if, and only if, $\epsilon \in \mathbb{R}_{>0}$. Note that in this paper, we suppose that the velocity cannot be measured, and therefore, the term $\digamma = \left[\digamma_x, \digamma_y\right]^T$ is actually unavailable for control design. To this end, we consider it as a part of uncertainties, and define the lumped disturbances δ_{lu} as $\delta_{lu} = \digamma + \delta_{tf}$, which will be estimated by an observation mechanism designed later. For the convenience of observer design, the following assumption is provided.

Assumption 4 (see other works [40–42]). *A bounded positive constant $B_{\delta_{lu}}$ exists such that the lumped disturbances δ_{lu} satisfy $\|\dot{\delta}_{lu}\| \leq B_{\delta_{lu}}$.*

Remark 3. From Equation (18), the original motion model for the underactuated airship has been transformed into a fully actuated uncertain Euler–Lagrange (EL) model, formally defined as $M(q)\,\ddot{q} + C(q, \dot{q})\,\dot{q} + G(q) = \tau$, where $q \in \mathbb{R}^n$ is the generalised coordinate, $M(q) \in \mathbb{R}^{n\times n}$ is the known matrix, $C(q, \dot{q}) \in \mathbb{R}^n$ is the known nonlinear dynamic, $G(q) \in \mathbb{R}^n$ accounts for uncertain dynamics and disturbances, and $\tau \in \mathbb{R}^n$ is the control variable; essentially, the EL model can describe various physical systems [33], such as robot manipulators [12, 24, 29] and spacecrafts [30, 31]. Thus, the presented method can be readily extended to a series of mechanical systems in second-order form.

Remark 4. It is emphasised that the coordinate transformation does not weaken the control quality; conversely, it is a potent approach to resolve the underactuated problem and realise the preassigned accuracy simultaneously. This is especially clear if we now construct a control algorithm that succeeds in forcing the signal $e_{t_1} = \varkappa_1 - \eta_d$ to shrink to zero within a finite time T_f and maintain it there for $t \geq T_f$, i.e., $\|e_{t_1}\| = 0, \forall t \geq T_f$, then the actual position error e will satisfy

$$\begin{aligned} \|e\| = \|\eta - \eta_d\| = \left\| \varkappa_1 - \epsilon \begin{bmatrix} \cos(\psi) \\ \sin(\psi) \end{bmatrix} - \eta_d \right\| = \left\| e_{t_1} - \epsilon \begin{bmatrix} \cos(\psi) \\ \sin(\psi) \end{bmatrix} \right\| \leq \|e_{t_1}\| \\ + \left\| \epsilon \begin{bmatrix} \cos(\psi) \\ \sin(\psi) \end{bmatrix} \right\| \leq \epsilon, \forall t \geq T_f. \end{aligned} \tag{20}$$

Evidently, decreasing ϵ yields a higher tracking precision.

Remark 5. It is necessary to remark that this paper views the airship as a rigid body and therefore the linear velocities u and v and the angular velocity r cannot change suddenly. In addition, the rate of change of the uncertainties δ is restrained as the stratospheric climate is stable and has limited energy. As a result, Assumption 4 is reasonable in reality and is widely employed in current literature [40–42] to facilitate the output feedback control realisation.

4.0 Main result

In this section, we first build an FTO to offer the exact information of the unmeasured velocity $\varkappa_2$ and the lumped disturbances δ_{lu} in an integrated manner. Afterward, in conjunction with the transformed model, the designed FTO, the backstepping technique, and the API method, a novel trajectory tracking control algorithm for stratospheric airships is proposed. Finally, a Lyapunov analysis is carried out to prove the closed-loop system stability.

https://doi.org/10.1017/aer.2022.47 Published online by Cambridge University Press

4.1 FTO

In this paper, the FTO is formulated by

$$\begin{cases} \dot{\hat{\varkappa}}_1 = \hat{\varkappa}_2 + p_1 sig^{r_1}\left(\varkappa_1 - \hat{\varkappa}_1\right) + q_1 sig^{z_1}\left(\varkappa_1 - \hat{\varkappa}_1\right) \\ \dot{\hat{\varkappa}}_2 = R(\psi)\, M_\epsilon \tau + \hat{\delta}_{lu} + p_2 sig^{r_2}\left(\varkappa_1 - \hat{\varkappa}_1\right) + q_2 sig^{z_2}\left(\varkappa_1 - \hat{\varkappa}_1\right) \\ \dot{\hat{\delta}}_{lu} = p_3 sig^{r_3}\left(\varkappa_1 - \hat{\varkappa}_1\right) + q_3 sig^{z_3}\left(\varkappa_1 - \hat{\varkappa}_1\right) + \Upsilon sign\left(\varkappa_1 - \hat{\varkappa}_1\right) \end{cases}, \tag{21}$$

where $\hat{\varkappa}_1$, $\hat{\varkappa}_2$, and $\hat{\delta}_{lu}$ are the estimates of $\varkappa_1$, $\varkappa_2$, and δ_{lu}, respectively. The parameters in Equation (21) satisfy $0 < r_i < 1$, $z_i > 1$, $r_i = ir_0 - (i-1)$, $z_i = iz_0 - (i-1)$, $i = 1, 2, 3$, $0 < r_0 < 1 - \sigma_1$, $0 < z_0 < 1 + \sigma_2$, $\sigma_1 \in \mathbb{R}_{>0}$ and $\sigma_2 \in \mathbb{R}_{>0}$ are sufficiently small constants, and $\Upsilon \geq B_{\delta_{lu}}$. The observer gains are selected to ensure the matrices

$$P = \begin{bmatrix} -p_1 & 1 & 0 \\ -p_2 & 0 & 1 \\ -p_3 & 0 & 0 \end{bmatrix} \text{ and } Q = \begin{bmatrix} -q_3 & 1 & 0 \\ -q_3 & 0 & 1 \\ -q_3 & 0 & 0 \end{bmatrix} \tag{22}$$

are Hurwitz. Based on the above contents, we obtained the main results of the FTO.

Theorem 1. *Using the FTO (21) under Assumption 4, the velocity $\varkappa_2$ and the lumped disturbances δ_{lu} can be estimated accurately; more specifically, the estimation errors e_{o_1}, e_{o_2}, and e_{o_3} can be driven to zero with a finite reaching time T_o.*

Proof of Theorem 1. Define $e_{o_1} = \varkappa_1 - \hat{\varkappa}_1$, $e_{o_2} = \varkappa_2 - \hat{\varkappa}_2$, and $e_{o_3} = \delta_{lu} - \hat{\delta}_{lu}$ as observer errors; therefore, together with Equation (18), the observer error dynamics can be computed as

$$\begin{cases} \dot{e}_{o_1} = e_{o_2} - p_1 sig^{r_1}\left(e_{o_1}\right) - q_1 sig^{z_1}\left(e_{o_1}\right) \\ \dot{e}_{o_2} = e_{o_3} - p_2 sig^{r_2}\left(e_{o_1}\right) - q_2 sig^{z_2}\left(e_{o_1}\right) \\ \dot{e}_{o_3} = \dot{\delta}_{lu} - p_3 sig^{r_3}\left(e_{o_1}\right) - q_3 sig^{z_3}\left(e_{o_1}\right) - \Upsilon sign\left(e_{o_1}\right) \end{cases}. \tag{23}$$

The reminder of this proof is quite similar to that of Theorem 1 given by Basin et al. [43], and therefore, it is omitted here for space.

Remark 6. The FTO (21) essentially is a uniform robust exact differentiator. Historically, the concept of uniform exact convergence was proposed by Cruz-Zavala et al. [44] for the first time. Note that chattering, measurement noise, sampling step and small delay are out of the scope of this paper.

4.2 Control algorithm design

The entire design procedure is elaborated as follows.

Step 1. Design a stabilising function for e_{t_1}. To begin with, let

$$e_{t_2} = \varkappa_2 - \dot{\eta}_d, e_{t_2}^{\dagger} = \hat{\varkappa}_2 - \dot{\eta}_d. \tag{24}$$

Consider the simple quadratic Lyapunov function candidate $V_1 = \frac{1}{2} e_{t_1}^T e_{t_1}$. Evaluating the time derivative of V_1 by using Equations (18) and (24) results in

$$\dot{V}_1 = e_{t_1}^T e_{t_2} = e_{t_1}^T (\varkappa_2 - \dot{\eta}_d) = e_{t_1}^T \left(\hat{\varkappa}_2 + e_{o_2} - \dot{\eta}_d\right) = e_{t_1}^T e_{t_2}^{\dagger} + e_{t_1}^T e_{o_2}. \tag{25}$$

Adopting the virtual control law

$$e_{t_2}^* = -\lfloor \kappa_1 \rceil sig^{\alpha}\left(e_{t_1}\right) \tag{26}$$

for e_{t_1} produces

$$\dot{V}_1 = e_{t_1}^T\left(e_{t_2}^\dagger - e_{t_2}^*\right) - e_{t_1}^T \lfloor \kappa_1 \rceil sig^\alpha\left(e_{t_1}\right) + e_{t_1}^T e_{o_2} = e_{t_1}^T\left(e_{t_2}^\dagger - e_{t_2}^*\right) - \sum_{i=1}^{2} \kappa_{1_i} \left|e_{t_{1_i}}\right|^{1+\alpha} + e_{t_1}^T e_{o_2}, \tag{27}$$

where $\kappa_1 \in \mathbb{R}^2$ and $\alpha \in (0, 1)$. Define the intermediate variable ϖ as

$$\varpi = sig^{\frac{1}{\alpha}}\left(e_{t_2}^\dagger\right) - sig^{\frac{1}{\alpha}}\left(e_{t_2}^*\right), \tag{28}$$

and together with Lemma 4, we get

$$\begin{aligned} e_{t_1}^T\left(e_{t_2}^\dagger - e_{t_2}^*\right) &= \sum_{i=1}^{2} e_{t_{1_i}}\left(e_{t_{2_i}}^\dagger - e_{t_{2_i}}^*\right) \le \sum_{i=1}^{2} \left|e_{t_{1_i}}\right| \left|e_{t_{2_i}}^\dagger - e_{t_{2_i}}^*\right| \\ &= \sum_{i=1}^{2} \left|e_{t_{1_i}}\right| \left|sig^\alpha\left(sig^{\frac{1}{\alpha}}\left(e_{t_{2_i}}^\dagger\right)\right) - sig^\alpha\left(sig^{\frac{1}{\alpha}}\left(e_{t_{2_i}}^*\right)\right)\right| \\ &\le \sum_{i=1}^{2} 2^{1-\alpha} \left|e_{t_{1_i}}\right| \left|sig^{\frac{1}{\alpha}}\left(e_{t_{2_i}}^\dagger\right) - sig^{\frac{1}{\alpha}}\left(e_{t_{2_i}}^*\right)\right|^\alpha \le \sum_{i=1}^{2} 2^{1-\alpha} \left|e_{t_{1_i}}\right| \left|\varpi_i\right|^\alpha. \end{aligned} \tag{29}$$

In view of Lemma 2, Equation (29) can be rewritten as

$$e_{t_1}^T\left(\bar{e}_{t_2} - \bar{e}_{t_2}^*\right) \le \sum_{i=1}^{2} \left(\frac{2^{1-\alpha}}{1+\alpha} \left|e_{t_{1_i}}\right|^{1+\alpha} + \frac{2^{1-\alpha}\alpha}{1+\alpha} \left|\varpi_i\right|^{1+\alpha}\right). \tag{30}$$

Substituting Equation (30) for Equation (27), the derivative $\dot{V}_1$ becomes

$$\dot{V}_1 \le -\sum_{i=1}^{2} \left(\kappa_{1_i} - \frac{2^{1-\alpha}}{1+\alpha}\right) \left|e_{t_{1_i}}\right|^{1+\alpha} + \sum_{i=1}^{2} \frac{2^{1-\alpha}\alpha}{1+\alpha} \left|\varpi_i\right|^{1+\alpha} + e_{t_1}^T e_{o_2}. \tag{31}$$

Step 2. Design a fixed-time control law for τ. To this end, select the complete Lyapunov function candidate as

$$V = V_1 + \sum_{i=1}^{2} V_{2_i}, \tag{32}$$

where V_{2_i}, $i = 1, 2$, takes the form

$$V_{2_i} = \int_{e_{t_{2_i}}^*}^{e_{t_{2_i}}^\dagger} sig^{2-\alpha}\left(sig^{\frac{1}{\alpha}}(s) - sig^{\frac{1}{\alpha}}\left(e_{t_{2_i}}^*\right)\right) ds. \tag{33}$$

In the sequel, we demonstrate that V_{2_i} is a scalar positive function through analysing the following cases.

- **Case 1:** $e_{t_{2_i}}^\dagger > e_{t_{2_i}}^* \ge 0$. From $sig^\iota(\cdot) = |\cdot|^\iota sign(\cdot)$ and $s \in \left[e_{t_{2_i}}^\dagger, e_{t_{2_i}}^*\right]$ we thus get

  $$s \ge e_{t_{2_i}}^* \ge 0, \quad sig^{\frac{1}{\alpha}}(s) = s^{\frac{1}{\alpha}}, \quad \text{and} \quad sig^{\frac{1}{\alpha}}\left(e_{t_{2_i}}^*\right) = e_{t_{2_i}}^{*\frac{1}{\alpha}}. \tag{34}$$

  This implies that

  $$V_{2_i} = \int_{e_{t_{2_i}}^*}^{e_{t_{2_i}}^\dagger} \left|s^{\frac{1}{\alpha}} - e_{t_{2_i}}^{*\frac{1}{\alpha}}\right|^{2-\alpha} sign\left(s^{\frac{1}{\alpha}} - e_{t_{2_i}}^{*\frac{1}{\alpha}}\right) ds = \int_{e_{t_{2_i}}^*}^{e_{t_{2_i}}^\dagger} \left(s^{\frac{1}{\alpha}} - e_{t_{2_i}}^{*\frac{1}{\alpha}}\right)^{2-\alpha} ds, \tag{35}$$

  where we used the fact that the power function $f(x) = x^{\frac{1}{\alpha}}$ is strictly increasing when $x > 0$. This, together with the well-known mean value theorem, gives

  $$V_{2_i} = \left(s_1^{*\frac{1}{\alpha}} - e_{t_{2_i}}^{*\frac{1}{\alpha}}\right)^{2-\alpha} \left(e_{t_{2_i}}^\dagger - e_{t_{2_i}}^*\right) > 0 \tag{36}$$

  with $s_1^* \in \left(e_{t_{2_i}}^*, e_{t_{2_i}}^\dagger\right)$.

https://doi.org/10.1017/aer.2022.47 Published online by Cambridge University Press

- **Case 2:** $e^{\dagger}_{t_{2_i}} \geq 0 > e^{*}_{t_{2_i}}$. Rewrite Equation (33) as

$$V_{2_i} = \int_0^{e^{\dagger}_{t_{2_i}}} sig^{2-\alpha}\left(sig^{\frac{1}{\alpha}}(s) - sig^{\frac{1}{\alpha}}\left(e^{*}_{t_{2_i}}\right)\right) ds + \int_{e^{*}_{t_{2_i}}}^{0} sig^{2-\alpha}\left(sig^{\frac{1}{\alpha}}(s) - sig^{\frac{1}{\alpha}}\left(e^{*}_{t_{2_i}}\right)\right) ds. \quad (37)$$

Regarding the first term on the right side of Equation (37), if $e^{\dagger}_{t_{2_i}} = 0$, then $\int_0^{e^{\dagger}_{t_{2_i}}} sig^{2-\alpha}\left(sig^{\frac{1}{\alpha}}(s) - sig^{\frac{1}{\alpha}}\left(e^{*}_{t_{2_i}}\right)\right) ds = 0$. Otherwise, we can easily verify that there exists a strictly positive constant $s^{*}_2 \in \left(0, e^{\dagger}_{t_{2_i}}\right)$ such that

$$\begin{aligned}&\int_0^{e^{\dagger}_{t_{2_i}}} sig^{2-\alpha}\left(sig^{\frac{1}{\alpha}}(s) - sig^{\frac{1}{\alpha}}\left(e^{*}_{t_{2_i}}\right)\right) ds = \int_0^{e^{\dagger}_{t_{2_i}}} \left|s^{\frac{1}{\alpha}} + \left|e^{*}_{t_{2_i}}\right|^{\frac{1}{\alpha}}\right|^{2-\alpha} sign\left(s^{\frac{1}{\alpha}} + \left|e^{*}_{t_{2_i}}\right|^{\frac{1}{\alpha}}\right) ds = \\ &\int_0^{e^{\dagger}_{t_{2_i}}} \left(s^{\frac{1}{\alpha}} + \left|e^{*}_{t_{2_i}}\right|^{\frac{1}{\alpha}}\right)^{2-\alpha} ds = \left(s_2^{*\frac{1}{\alpha}} + \left|e^{*}_{t_{2_i}}\right|^{\frac{1}{\alpha}}\right)^{2-\alpha} e^{\dagger}_{t_{2_i}} > 0,\end{aligned} \quad (38)$$

where $e^{*}_{t_{2_i}} < 0 \Rightarrow sign\left(e^{*}_{t_{2_i}}\right) = -1, \forall s \in \left[0, e^{\dagger}_{t_{2_i}}\right] \Rightarrow sign(s) = 1$, and the mean value theorem have been used.

As for the second term, let us now consider the integration by substitution technique. By making the substitution $s = -g$, we have

$$\begin{aligned}&\int_{e^{*}_{t_{2_i}}}^{0} sig^{2-\alpha}\left(sig^{\frac{1}{\alpha}}(s) - sig^{\frac{1}{\alpha}}\left(e^{*}_{t_{2_i}}\right)\right) ds = \int_0^{\left|e^{*}_{t_{2_i}}\right|} sig^{2-\alpha}\left(sig^{\frac{1}{\alpha}}(-g) - sig^{\frac{1}{\alpha}}\left(e^{*}_{t_{2_i}}\right)\right) dg = \\ &\int_0^{\left|e^{*}_{t_{2_i}}\right|} sig^{2-\alpha}\left(|g|^{\frac{1}{\alpha}} sign(-g) - \left|e^{*}_{t_{2_i}}\right|^{\frac{1}{\alpha}} sign\left(e^{*}_{t_{2_i}}\right)\right) dg.\end{aligned} \quad (39)$$

Further consider that $sign\left(e^{*}_{t_{2_i}}\right) = -1$ and $\forall g \in \left[0, \left|e^{*}_{t_{2_i}}\right|\right]$ means $sign(-g) = -1$ and $\left|e^{*}_{t_{2_i}}\right|^{\frac{1}{\alpha}} > |g|^{\frac{1}{\alpha}}$. Consequently, Equation (39) simply becomes

$$\begin{aligned}&\int_0^{\left|e^{*}_{t_{2_i}}\right|} sig^{2-\alpha}\left(|g|^{\frac{1}{\alpha}} sign(-g) - \left|e^{*}_{t_{2_i}}\right|^{\frac{1}{\alpha}} sign\left(e^{*}_{t_{2_i}}\right)\right) dg = \int_0^{\left|e^{*}_{t_{2_i}}\right|} sig^{2-\alpha}\left(\left|e^{*}_{t_{2_i}}\right|^{\frac{1}{\alpha}} - |g|^{\frac{1}{\alpha}}\right) dg = \\ &\int_0^{\left|e^{*}_{t_{2_i}}\right|} \left(\left|e^{*}_{t_{2_i}}\right|^{\frac{1}{\alpha}} - |g|^{\frac{1}{\alpha}}\right)^{2-\alpha} sign\left(\left|e^{*}_{t_{2_i}}\right|^{\frac{1}{\alpha}} - |g|^{\frac{1}{\alpha}}\right) dg = \int_0^{\left|e^{*}_{t_{2_i}}\right|} \left(\left|e^{*}_{t_{2_i}}\right|^{\frac{1}{\alpha}} - |g|^{\frac{1}{\alpha}}\right)^{2-\alpha} dg.\end{aligned} \quad (40)$$

Proceeding similarly to get Equation (36) leads to

$$\int_{e^{*}_{t_{2_i}}}^{0} sig^{2-\alpha}\left(sig^{\frac{1}{\alpha}}(s) - sig^{\frac{1}{\alpha}}\left(e^{*}_{t_{2_i}}\right)\right) ds = \left(\left|e^{*}_{t_{2_i}}\right|^{\frac{1}{\alpha}} - g_1^{*\frac{1}{\alpha}}\right)^{2-\alpha} \left|e^{*}_{t_{2_i}}\right| > 0 \quad (41)$$

with $g^{*}_1 \in \left(0, \left|e^{*}_{t_{2_i}}\right|\right)$. Summarising the results in Equations (38) and (41) gives $V_{2_i} > 0$ in the case of $e^{\dagger}_{t_{2_i}} \geq 0 > e^{*}_{t_{2_i}}$.

- **Case 3:** $0 \geq e^{\dagger}_{t_{2_i}} > e^{*}_{t_{2_i}}$. Clearly, in this case, $0 \leq \left|e^{\dagger}_{t_{2_i}}\right| < \left|e^{*}_{t_{2_i}}\right|$ holds. Let us again use the integration by substitution technique. Setting $s = -g$ results in

$$V_{2_i} = \int_{e^{*}_{t_{2_i}}}^{e^{\dagger}_{t_{2_i}}} sig^{2-\alpha}\left(sig^{\frac{1}{\alpha}}(s) - sig^{\frac{1}{\alpha}}\left(e^{*}_{t_{2_i}}\right)\right) ds = \int_{\left|e^{\dagger}_{t_{2_i}}\right|}^{\left|e^{*}_{t_{2_i}}\right|} sig^{2-\alpha}\left(sig^{\frac{1}{\alpha}}(-g) - sig^{\frac{1}{\alpha}}\left(e^{*}_{t_{2_i}}\right)\right) dg. \quad (42)$$

https://doi.org/10.1017/aer.2022.47 Published online by Cambridge University Press

Following the same lines to obtain Equations (40) and (41), it can also be shown that

$$V_{2_i} = \int_{\left|e^\dagger_{t_{2_i}}\right|}^{\left|e^*_{t_{2_i}}\right|} \left(\left|e^*_{t_{2_i}}\right|^{\frac{1}{\alpha}} - |g|^{\frac{1}{\alpha}}\right)^{2-\alpha} dg = \left(\left|e^*_{t_{2_i}}\right|^{\frac{1}{\alpha}} - g_2^{*\frac{1}{\alpha}}\right)^{2-\alpha} \left(\left|e^*_{t_{2_i}}\right| - \left|e^\dagger_{t_{2_i}}\right|\right) > 0 \tag{43}$$

with $g_2^* \in \left(\left|e^\dagger_{t_{2_i}}\right|, \left|e^*_{t_{2_i}}\right|\right)$.

- **Case 4:** $e^*_{t_{2_i}} \geq 0 > e^\dagger_{t_{2_i}}$. We now switch the upper and lower bounds of integral (33) and thus obtain

$$\begin{aligned} V_{2_i} &= -\int_{e^\dagger_{t_{2_i}}}^{e^*_{t_{2_i}}} sig^{2-\alpha}\left(sig^{\frac{1}{\alpha}}(s) - sig^{\frac{1}{\alpha}}\left(e^*_{t_{2_i}}\right)\right) ds \\ &= -\int_{0}^{e^*_{t_{2_i}}} sig^{2-\alpha}\left(sig^{\frac{1}{\alpha}}(s) - sig^{\frac{1}{\alpha}}\left(e^*_{t_{2_i}}\right)\right) ds - \int_{e^\dagger_{t_{2_i}}}^{0} sig^{2-\alpha}\left(sig^{\frac{1}{\alpha}}(s) - sig^{\frac{1}{\alpha}}\left(e^*_{t_{2_i}}\right)\right) ds. \end{aligned} \tag{44}$$

The first term on the right side of Equation (44) is identically equal to zero if $e^*_{t_{2_i}} = 0$; if not, proceeding as before, it can be simplified as

$$\begin{aligned} &-\int_{0}^{e^*_{t_{2_i}}} sig^{2-\alpha}\left(sig^{\frac{1}{\alpha}}(s) - sig^{\frac{1}{\alpha}}\left(e^*_{t_{2_i}}\right)\right) ds = -\int_{0}^{e^*_{t_{2_i}}} \left|s^{\frac{1}{\alpha}} - e^{*\frac{1}{\alpha}}_{t_{2_i}}\right|^{2-\alpha} sign\left(s^{\frac{1}{\alpha}} - e^{*\frac{1}{\alpha}}_{t_{2_i}}\right) ds = \\ &\left(e^{*\frac{1}{\alpha}}_{t_{2_i}} - s_3^{*\frac{1}{\alpha}}\right)^{2-\alpha} e^*_{t_{2_i}} > 0, \end{aligned} \tag{45}$$

where $s_3^* \in \left(0, e^\dagger_{t_{2_i}}\right)$ and we have used the fact $\forall s \in \left[0, e^*_{t_{2_i}}\right] \Rightarrow s^{\frac{1}{\alpha}} \leq e^{*\frac{1}{\alpha}}_{t_{2_i}}$.
And the second term, given the substitution $s = -g$, satisfies

$$\begin{aligned} &-\int_{e^\dagger_{t_{2_i}}}^{0} sig^{2-\alpha}\left(sig^{\frac{1}{\alpha}}(s) - sig^{\frac{1}{\alpha}}\left(e^*_{t_{2_i}}\right)\right) ds = \int_{\left|e^\dagger_{t_{2_i}}\right|}^{0} sig^{2-\alpha}\left(sig^{\frac{1}{\alpha}}(-g) - sig^{\frac{1}{\alpha}}\left(e^*_{t_{2_i}}\right)\right) dg = \\ &-\int_{0}^{\left|e^\dagger_{t_{2_i}}\right|} sig^{2-\alpha}\left(sig^{\frac{1}{\alpha}}(-g) - sig^{\frac{1}{\alpha}}\left(e^*_{t_{2_i}}\right)\right) dg = \int_{0}^{\left|e^\dagger_{t_{2_i}}\right|} \left(g^{\frac{1}{\alpha}} + \left|e^*_{t_{2_i}}\right|^{\frac{1}{\alpha}}\right)^{2-\alpha} dg = \\ &\left(g_3^{*\frac{1}{\alpha}} + \left|e^*_{t_{2_i}}\right|^{\frac{1}{\alpha}}\right)^{2-\alpha} \left|e^\dagger_{t_{2_i}}\right| > 0, \end{aligned} \tag{46}$$

where $g_3^* \in \left(0, \left|e^*_{t_{2_i}}\right|\right)$ and we have used the facts $sign(-g) = -1$ and $sign\left(e^*_{t_{2_i}}\right) = -1$. Taking Equations (44) and (45) into account, we know that $V_{2_i} > 0$ when $e^*_{t_{2_i}} \geq 0 > e^\dagger_{t_{2_i}}$.

Evidently, the above discussion guarantees that V_{2_i} is positively defined. Differentiating V_{2_i} with respect to time and applying Lemma 5 lead to

$$\dot{V}_{2_i} = sig^{2-\alpha}(\varpi_i)\, \dot{e}^\dagger_{t_{2_i}} - (2-\alpha) \frac{\mathrm{d}sig^{\frac{1}{\alpha}}\left(e^*_{t_{2_i}}\right)}{\mathrm{d}t} \int_{e^*_{t_{2_i}}}^{e^\dagger_{t_{2_i}}} \left|sig^{\frac{1}{\alpha}}(s) - sig^{\frac{1}{\alpha}}\left(e^*_{t_{2_i}}\right)\right|^{1-\alpha} ds. \tag{47}$$

Noting that

$$sig^{\frac{1}{\alpha}}\left(\kappa_{1_i} sig^{\alpha}\left(e_{t_{1_i}}\right)\right) = \kappa_{1_i}^{\frac{1}{\alpha}} \left|\, \left|e_{t_{1_i}}\right|^{\alpha} sign\left(e_{t_{1_i}}\right) \right|^{\frac{1}{\alpha}} sign\left(\left|e_{t_{1_i}}\right|^{\alpha} sign\left(e_{t_{1_i}}\right)\right) = \kappa_{1_i}^{\frac{1}{\alpha}} e_{t_{1_i}} \tag{48}$$

and

$$\frac{\mathrm{d}sig^{\frac{1}{\alpha}}\left(e^*_{t_{2_i}}\right)}{\mathrm{d}t} = -\frac{\mathrm{d}sig^{\frac{1}{\alpha}}\left(\kappa_{1_i} sig^{\alpha}\left(e_{t_{1_i}}\right)\right)}{\mathrm{d}e_{t_{1_i}}} e_{t_{2_i}} = -\kappa_{1_i}^{\frac{1}{\alpha}} e_{t_{2_i}}, \tag{49}$$

we have

$$\dot{V}_{2_i} = sig^{2-\alpha}(\varpi_i)\, \dot{e}^\dagger_{t_{2_i}} + \kappa_{1_i}^{\frac{1}{\alpha}} (2-\alpha)\, e_{t_{2_i}} \int_{e^*_{t_{2_i}}}^{e^\dagger_{t_{2_i}}} \left|sig^{\frac{1}{\alpha}}(s) - sig^{\frac{1}{\alpha}}\left(e^*_{t_{2_i}}\right)\right|^{1-\alpha} ds. \tag{50}$$

https://doi.org/10.1017/aer.2022.47 Published online by Cambridge University Press

The second term in the right side of Equation (50) satisfies

$$\begin{aligned}&\left|\kappa_{1_i}^{\frac{1}{\alpha}}(2-\alpha)\,e_{t_{2_i}}\int_{e^*_{t_{2_i}}}^{e^\dagger_{t_{2_i}}}\right|sig^{\frac{1}{\alpha}}(s)-sig^{\frac{1}{\alpha}}\left(e^*_{t_{2_i}}\right)|^{1-\alpha}ds|\\&\le\kappa_{1_i}^{\frac{1}{\alpha}}(2-\alpha)\left|e_{t_{2_i}}\right|\left|e^\dagger_{t_{2_i}}-e^*_{t_{2_i}}\right|\left|sig^{\frac{1}{\alpha}}\left(e^\dagger_{t_{2_i}}\right)-sig^{\frac{1}{\alpha}}\left(e^*_{t_{2_i}}\right)\right|^{1-\alpha}\\&\le\kappa_{1_i}^{\frac{1}{\alpha}}(2-\alpha)\left|e_{t_{2_i}}\right|\left|sig^{\alpha}\left(sig^{\frac{1}{\alpha}}\left(e^\dagger_{t_{2_i}}\right)\right)-sig^{\alpha}\left(sig^{\frac{1}{\alpha}}\left(e^*_{t_{2_i}}\right)\right)\right|\times\left|sig^{\frac{1}{\alpha}}\left(e^\dagger_{t_{2_i}}\right)-sig^{\frac{1}{\alpha}}\left(e^*_{t_{2_i}}\right)\right|^{1-\alpha}\\&\le\kappa_{1_i}^{\frac{1}{\alpha}}(2-\alpha)\,2^{1-\alpha}\left|e_{t_{2_i}}\right||\varpi_i|\end{aligned}\tag{51}$$

with

$$\begin{aligned}\left|e_{t_{2_i}}\right|=\left|e^\dagger_{t_{2_i}}+e_{o_{2_i}}\right|&\le\left|e^\dagger_{t_{2_i}}\right|+\left|e_{o_{2_i}}\right|\le|e^\dagger_{t_{2_i}}-e^*_{t_{2_i}}|+|\kappa_{1_i}sig^{\alpha}\left(e_{t_{1_i}}\right)|+\left|e_{o_{2_i}}\right|\\&\le|sig^{\alpha}\left(sig^{\frac{1}{\alpha}}\left(e^\dagger_{t_{2_i}}\right)\right)-sig^{\alpha}\left(sig^{\frac{1}{\alpha}}\left(e^*_{t_{2_i}}\right)\right)|+\kappa_{1_i}\left|e_{t_{1_i}}\right|^{\alpha}+\left|e_{o_{2_i}}\right|\\&\le2^{1-\alpha}|\varpi_i|^{\alpha}+\kappa_{1_i}\left|e_{t_{1_i}}\right|^{\alpha}+\left|e_{o_{2_i}}\right|,\end{aligned}\tag{52}$$

where Equations (24), and (26), (28), and Lemma 4 have been used. Coupling Equations (51) and (52), we have

$$\begin{aligned}&\left|\kappa_{1_i}^{\frac{1}{\alpha}}(2-\alpha)\,e_{t_{2_i}}\int_{e^*_{t_{2_i}}}^{e^\dagger_{t_{2_i}}}\right|sig^{\frac{1}{\alpha}}(s)-sig^{\frac{1}{\alpha}}\left(e^*_{t_{2_i}}\right)|^{1-\alpha}ds|\\&\le\kappa_{1_i}^{\frac{1}{\alpha}}(2-\alpha)\,2^{1-\alpha}|\varpi_i|\left(2^{1-\alpha}|\varpi_i|^{\alpha}+\kappa_{1_i}\left|e_{t_{1_i}}\right|^{\alpha}+\left|e_{o_{2_i}}\right|\right)\\&=\kappa_{1_i}^{\frac{1}{\alpha}}(2-\alpha)\,2^{2-2\alpha}|\varpi_i|^{1+\alpha}+\kappa_{1_i}^{1+\frac{1}{\alpha}}(2-\alpha)\,2^{1-\alpha}|\varpi_i|\left|e_{t_{1_i}}\right|^{\alpha}+\kappa_{1_i}^{\frac{1}{\alpha}}(2-\alpha)\,2^{1-\alpha}|\varpi_i|\left|e_{o_{2_i}}\right|\\&\le\kappa_{1_i}^{\frac{1}{\alpha}}(2-\alpha)\,2^{2-2\alpha}|\varpi_i|^{1+\alpha}+\frac{(2-\alpha)\,2^{1-\alpha}\alpha}{1+\alpha}\left|e_{t_{1_i}}\right|^{1+\alpha}+\frac{(2-\alpha)\,2^{1-\alpha}}{1+\alpha}\kappa_{1_i}^{1+\alpha}|\varpi_i|^{1+\alpha}\\&+\kappa_{1_i}^{\frac{1}{\alpha}}(2-\alpha)\,2^{1-\alpha}|\varpi_i|\left|e_{o_{2_i}}\right|,\end{aligned}\tag{53}$$

where Lemma 2 has been used. Then, the differentiation of V_{2_i} and the utilisation of Equation (53) yield

$$\begin{aligned}\dot V_{2i}\le{}&sig^{2-\alpha}(\varpi_i)\,\dot e^\dagger_{t_{2_i}}+\frac{(2-\alpha)\,2^{1-\alpha}\alpha}{1+\alpha}\left|e_{t_{1_i}}\right|^{1+\alpha}\\&+\left(\kappa_{1_i}^{\frac{1}{\alpha}}(2-\alpha)\,2^{2-2\alpha}+\frac{(2-\alpha)\,2^{1-\alpha}}{1+\alpha}\kappa_{1_i}^{1+\alpha}\right)|\varpi_i|^{1+\alpha}+\kappa_{1_i}^{\frac{1}{\alpha}}(2-\alpha)\,2^{1-\alpha}|\varpi_i|\left|e_{o_{2_i}}\right|.\end{aligned}\tag{54}$$

Together with Equations (18), (23), (24), (27), and (54), the definition of V, and the dynamics of $e^\dagger_{t_2}$

$$\dot e^\dagger_{t_2}=R(\psi)\,M_\epsilon\tau+\delta_{lu}-\ddot\eta_d+p_2sig^{r_2}\left(e_{o_1}\right)+q_2sig^{z_2}\left(e_{o_1}\right)-e_{o_3},\tag{55}$$

we get

$$\begin{aligned}\dot V\le{}&-\sum_{i=1}^{2}\left(\kappa_{1_i}-\gamma_{1_i}\right)\left|e_{t_{1_i}}\right|^{1+\alpha}+\sum_{i=1}^{2}\frac{\alpha}{1+\alpha}\left|e_{o_{2_i}}\right|^{1+\frac{1}{\alpha}}+\sum_{i=1}^{2}\gamma_{2_i}|\varpi_i|^{1+\alpha}+\sum_{i=1}^{2}\kappa_{1_i}^{\frac{1}{\alpha}}(2-\alpha)\,2^{1-\alpha}|\varpi_i|\left|e_{o_{2_i}}\right|\\&+\left(sig^{2-\alpha}(\varpi)\right)^T\left(R(\psi)\,M_\epsilon\tau+\delta_{lu}-\ddot\eta_d+p_2sig^{r_2}\left(e_{o_1}\right)+q_2sig^{z_2}\left(e_{o_1}\right)-e_{o_3}\right)\end{aligned}\tag{56}$$

with $\gamma_{1_i}=\frac{2^{1-\alpha}(1+(2-\alpha)\alpha)+1}{1+\alpha}$ and $\gamma_{2_i}=\frac{2^{1-\alpha}\alpha}{1+\alpha}+\kappa_{1_i}^{\frac{1}{\alpha}}(2-\alpha)\,2^{2-2\alpha}+\frac{(2-\alpha)2^{1-\alpha}}{1+\alpha}\kappa_{1_i}^{1+\alpha}$, $i=1,2$. According to the structure of $\dot V$, the trajectory tracking control law for τ is designed as

$$\tau=-M_\epsilon^{-1}R^{-1}(\psi)\left(\hat\delta_{lu}-\ddot\eta_d+(\lfloor\kappa_2\rceil+\lfloor\gamma_2\rceil)\,sig^{2\alpha-1}(\varpi)+\varrho(t)\left(sig^{\alpha}(\varpi)+sig^{2-\alpha}(\varpi)\right)\right),\tag{57}$$

https://doi.org/10.1017/aer.2022.47 Published online by Cambridge University Press

where $\rho(t)=\begin{cases}((T_\rho-t)/T_\rho)^{\frac{1}{\alpha_\rho}}(\rho_0-\rho_\infty)+\rho_\infty & ,0\le t\le T_\rho\\ \rho_\infty & ,t>T_\rho\end{cases}$ with $\{\rho_0,\rho_\infty,\alpha_\rho,T_\rho\}\in\mathbb{R}_{>0}$, and $\kappa_2\in\mathbb{R}^2_{>0}$. The main results of this brief are included in the following theorem.

Theorem 2. *Consider the stratospheric airship (8) subject to underactuated dynamics, unmeasured velocities, modeling imperfections, and exogenous disturbances, with the coordinate transformation (11), the FTO (21), the virtual control law (26), and the control action (57). Suppose that Assumptions 1–4 hold and the control parameters are selected such that*

$$\kappa_{1_i}>\gamma_{1_i}+\kappa'_{1_i},\tag{58}$$

where $\kappa'_{1_i}\in R_{>0}$, $i=1,2$. Then, the position error $e=\eta-\eta_d$ converges to a preassigned small vicinity of the origin within a finite time T_f, while all the closed-loop states maintain bounded for $\forall t\ge 0$.

Proof of Theorem 2. Let us prove first that these signals do not go to infinity when $t\in[0,T_o]$. Substituting the control action (57) with design parameters satisfying the condition (58), we have

$$\begin{aligned}\dot V\le&-\sum_{i=1}^{2}\kappa'_{1_i}|e_{t_{2_i}}|^{1+\alpha}-\sum_{i=1}^{2}\kappa_{2i}|\varpi_i|^{1+\alpha}+\sum_{i=1}^{2}\kappa_{1_i}^{\frac{1}{\alpha}}(2-\alpha)\,2^{1-\alpha}|\varpi_i|\left|e_{o_{2_i}}\right|+\sum_{i=1}^{2}\frac{\alpha}{1+\alpha}\left|e_{o_{2_i}}\right|^{1+\frac{1}{\alpha}}\\&+\left(sig^{2-\alpha}(\varpi)\right)^T\left(p_2sig^{r_2}\left(e_{o_1}\right)+q_2sig^{z_2}\left(e_{o_1}\right)\right)-\varrho(t)\left(sig^{2-\alpha}(\varpi)\right)^T\left(sig^{\alpha}(\varpi)+sig^{2-\alpha}(\varpi)\right),\end{aligned}\tag{59}$$

where the fact

$$sig^{2\alpha-1}(\varpi_i)\,sig^{2-\alpha}(\varpi_i)=|\varpi_i|^{1+\alpha}\tag{60}$$

has been used. Noticing that the signals e_{o_1} and e_{o_2} decay to zero after a fixed-time time T_0, hence $\{e_{o_{1_i}},e_{o_{2_i}}\}\in\mathbb{L}^\infty$. Accordingly, there exists a constant $B_{e_o}\in\mathbb{R}_{>0}$ such that $\sup_{t\in[0,\infty)}\{|e_{o_{1_i}}|,\left|e_{o_{2_i}}\right|,|e_{o_{1_i}}|^{r_2},\left|e_{o_{2_i}}\right|^{z_2}\}\le B_{e_o}$, $i=1,2$. This, combined with Young's inequality, gives

$$\sum_{i=1}^{2}\kappa_{1_i}^{\frac{1}{\alpha}}(2-\alpha)\,2^{1-\alpha}|\varpi_i||e_{o_{1_i}}|\le\sum_{i=1}^{2}\left(\varrho(t)\,|\varpi_i|^2+\frac{\kappa_{1_i}^{\frac{2}{\alpha}}(2-\alpha)^2\,2^{2-2\alpha}}{4\varrho(t)}B_{e_o}^2\right),\tag{61}$$

$$\left(sig^{2-\alpha}(\varpi)\right)^T\left(p_2sig^{r_2}\left(e_{o_1}\right)+q_2sig^{z_2}\left(e_{o_1}\right)\right)\le\sum_{i=1}^{2}\left(\varrho(t)\,|\varpi_i|^{4-2\alpha}+\frac{p_2^2+z_2^2}{4\varrho(t)}|B_{e_o}|^2\right).\tag{62}$$

In view of Equations (61) and (62), Equation (59) can be restated as

$$\begin{aligned}\dot V\le&-\sum_{i=1}^{2}\kappa'_{1_i}\left|e_{t_{1_i}}\right|^{1+\alpha}-\sum_{i=1}^{2}\kappa_{2i}|\varpi_i|^{1+\alpha}+\sum_{i=1}^{2}\frac{\alpha}{1+\alpha}B_{e_o}^{1+\frac{1}{\alpha}}+\sum_{i=1}^{2}\frac{\kappa_{1_i}^{\frac{2}{\alpha}}(2-\alpha)^2\,2^{2-2\alpha}}{4\varrho(t)}B_{e_o}^2\\&+\sum_{i=1}^{2}\frac{p_2^2+z_2^2}{4\varrho(t)}|B_{e_{on}}|^2.\end{aligned}\tag{63}$$

Apparently, a constant $B_s^{[0,T_o]}\in\mathbb{R}_{>0}$ exists, which is an upper bound on the sum of the last three terms in Equation (63) when $t\in[0,T_o]$. Besides, Recalling the definition of function V_{2i}, we can easily see

$$\begin{aligned}V_{2i}=&\int_{e^*_{t_{2_i}}}^{e^\dagger_{t_{2_i}}}sig^{2-\alpha}\left(sig^{\frac{1}{\alpha}}(s)-sig^{\frac{1}{\alpha}}\left(e^*_{t_{2_i}}\right)\right)ds\le\left|e^\dagger_{t_{2_i}}-e^*_{t_{2_i}}\right|\left|sig^{2-\alpha}\left(sig^{\frac{1}{\alpha}}\left(e^\dagger_{t_{2_i}}\right)-sig^{\frac{1}{\alpha}}\left(e^*_{t_{2_i}}\right)\right)\right|\\&\le|sig^{\alpha}\left(sig^{\frac{1}{\alpha}}\left(e^*_{t_{2_i}}\right)\right)-sig^{\alpha}\left(sig^{\frac{1}{\alpha}}\left(e^\dagger_{t_{2_i}}\right)\right)||\varpi_i|^{2-\alpha}\le 2^{1-\alpha}|\varpi_i|^2\le 2|\varpi_i|^2,\end{aligned}\tag{64}$$

and therefore the complete Lyapunov function candidate V satisfies $V\le 2e_{t_1}^Te_{t_1}+2\varpi^T\varpi$. Since $\alpha\in(0,1)\Rightarrow\frac{1+\alpha}{2}\in\left(\frac{1}{2},1\right)$, this further leads to

$$V^{\frac{1+\alpha}{2}}\le\left(2\sum_{i=1}^{2}e_{t_{1_i}}^2+2\sum_{i=1}^{2}\varpi_i^2\right)^{\frac{1+\alpha}{2}}\le 2^{\frac{1+\alpha}{2}}\sum_{i=1}^{2}\left|e_{t_{1_i}}\right|^{1+\alpha}+2^{\frac{1+\alpha}{2}}\sum_{i=1}^{2}|\varpi_i|^{1+\alpha}\tag{65}$$

https://doi.org/10.1017/aer.2022.47 Published online by Cambridge University Press

Table 1. *Airship model parameters*

Notation	Value	Notation	Value	Notation	Value
m_u (kg)	301	d_r (kg/s)	73	Δm_v (kg)	155
m_v (kg)	455	$\Delta\delta_u$	15	Δm_r (kg · m^2)	4,127
m_r (kg · m^2)	12,176	$\Delta\delta_v$	15	Δd_u (kg/s)	10
d_u (kg/s)	50	$\Delta\delta_r$	300	Δd_v (kg/s)	10
d_v (kg/s)	50	Δm_u (kg)	101	Δd_r (kg/s)	13

When $V > 1$, summarising the results in Equations (59), (63), (64) and (65) gives

$$\dot{V} \le -\lambda_0 V^{\frac{1+\alpha}{2}} + B_s^{[0,T_o]} \le -\lambda_0 V + B_s^{[0,T_o]}, \tag{66}$$

where Lemma 3 has been used, $\lambda_0 = \min\left(\frac{1}{2}\right)^{\frac{1+\alpha}{2}} \times \left\{\kappa'_{1_i}, \kappa_{2i}\right\}$, $i = 1, 2$. Multiplying Equation (66) by $e^{\lambda_0 t}$ and integrating it over $[0, t]$, we have

$$0 \le V(t) \le \left(V(0) - \frac{B_s^{[0,T_o]}}{\lambda_0}\right) e^{-\lambda_0 t} + \frac{B_s^{[0,T_o]}}{\lambda_0}. \tag{67}$$

Besides, in the case of $V \le 1$, the system states e_{t_i}, $i = 1, 2$, and ϖ are obviously bounded. As a result, we can conclude that these signals will not drift to infinity as $t \in [0, T_o]$.

Now, we proceed to prove Theorem 2. Theorem 1 reveals that $\hat{\varkappa}_2 = \varkappa_2$ and $\hat{\delta}_{lu} = \delta_{lu}$ for $\forall t \ge T_0$. Along with the fact that $\varrho(t) \in \mathbb{R}_{>0}$, Equation (59) becomes

$$\dot{V} \le -\sum_{i=1}^{2} \kappa'_{1_i} \left|e_{t_{1_i}}\right|^{1+\alpha} - \sum_{i=1}^{2} \kappa_{2i} |\varpi_i|^{1+\alpha} - \sum_{i=1}^{2} \varrho(t)\left(\left(|\varpi_i|^2 + |\varpi_i|^{4-2\alpha}\right)\right) \le -\lambda_0 V^{\frac{1+\alpha}{2}}, \tag{68}$$

Consequently, all of the system states remain bounded for $t \ge T_o$. Besides, it is noteworthy that:

1. the finite-time tracking task is fulfilled. Given Lemma 1, we can conclude that both e_{t_1} and ϖ decay to zero within a finite time T_f estimated by

$$T_f \le \frac{2V^{\frac{1-\alpha}{2}}(0)}{\lambda_0(1-\alpha)} + T_o; \tag{69}$$

2. a priori assignment of tracking accuracy is assured. Recalling Equation (20), we get

$$\|e_{t_1}\| = 0, \forall t \ge T_f \Rightarrow \max\{|x_e|, |y_e|\} \le \epsilon, \forall t \ge T_f, \tag{70}$$

   indicating that we can specify the accuracy bound with the parameter ϵ. □

Remark 7. In the related works on API method [30–35], the power is circumscribed to be an even integer or a ratio of two odd integers. However, with the benefit of Lemma 4, such curtailments are removed in our work.

Remark 8. In contrast to the sliding mode control designs [11, 14, 15, 42], the control action (57) is chattering-free. In this note, although the signum operator $sign(\cdot)$ is employed, the highly undesirable control activity is avoided as the fractional power term $sig^{\varsigma}(z) = |z|^{\varsigma} sign(z)$ is a non-smooth but continuous function of z, where $\varsigma > 0$. This is vital for the long-time flight of the airship as control chattering may shorten the lifespan of the devices. Moreover, from the definition of $\rho(t)$, we can find that $\rho(t)$ is a strictly decreasing positive function and it takes a very small value ρ_∞ when $t > T_\rho$. In this sense, we can avoid unnecessary control effort to some extent by incorporating it into the control action (57).

https://doi.org/10.1017/aer.2022.47 Published online by Cambridge University Press

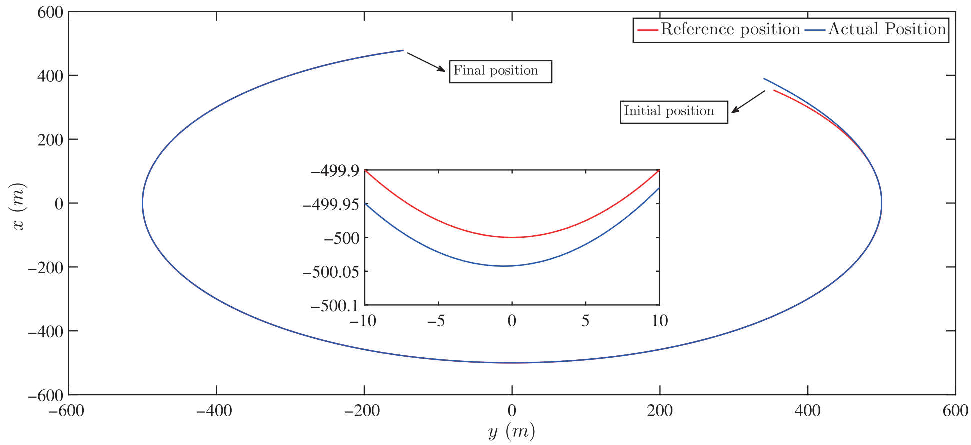

Figure 3. *Trajectories for horizontal tracking.*

5.0 Simulation

5.1 Simulation condition

In this section, numerical simulations are performed to intuitively evaluate the effectiveness of the preceding theoretical results with the running time $T_{final} = 100$s. The physical parameters of the stratospheric airship are borrowed from Zheng et al. [6] and Zhang et al. [18], and all of them are listed in Table 1.

In this simulations, the airship starts from $\left[x(0)\,, y(0)\right]^T = [340\text{m}, 390\text{m}]^T$ with initial heading $\psi(0) = 0.1$rad, and initial velocity $\nu(0) = [u(0)\,, v(0)\,, r(0)]^T = \left[0\text{m/s}, 0\text{m/s}, 0\text{rad/s}\right]^T$, and is required to track the reference trajectory

$$\eta_d = \begin{bmatrix} 500\sin\left(0.0052t + \dfrac{\pi}{4}\right) \\ 500\cos\left(0.0052t + \dfrac{\pi}{4}\right) \end{bmatrix}, \tag{71}$$

with the preassigned accuracy $\epsilon = 0.2$. To test the robustness, the disturbance δ_{dis} induced by environmental forces is mathematically assumed as [6, 10]:

$$\delta_{dis} = \begin{bmatrix} \delta_{dis_u} \\ \delta_{dis_v} \\ \delta_{dis_r} \end{bmatrix} = \begin{bmatrix} [1.4 + 2.1\sin(0.1t) + 1.1\cos(0.06t)] \times 40 \\ [-0.8 + 1.5\sin(0.1t) + 0.3\cos(0.06t)] \times 40 \\ -[2.3\sin(0.1t) + 1.9\cos(0.06t)] \times 110 \end{bmatrix}. \tag{72}$$

To fulfill this mission, the control parameters are selected as $p_1 = q_1 = 24$, $p_2 = q_2 = 216$, $p_3 = q_3 = 864$, $r_1 = 0.8$, $r_2 = 0.6$, $r_3 = 0.4$, $z_1 = 1.2$, $z_2 = 1.4$, $z_3 = 1.6$, $\Upsilon = 5$, $\epsilon = 0.2$, $\alpha = 0.7$, $\kappa_1 = [2, 2]^T$, $\kappa_2 = [0.1, 0.1]^T$, $\rho_0 = 1$, $\rho_\infty = 0.01$, $\alpha_\rho = 2$, and $T_\rho = 1$. The initial conditions of the FTO (21) are set to zero.

5.2 Simulation result

Applying the FTO (21) and the control action (57) to the airship model (8), we reach some simulation outcomes, illuminated by Figs 3-13. From Figs 3-6, we see that the airship can move to the desired trajectory swiftly and smoothly, and the position errors $x_e = x - x_d$ and $y_e = y - y_d$ decay toward a close vicinity of zero within a finite time. Then, the airship flies along the reference trajectory precisely, irrespective of underactuated dynamics, modeling imprecisions, and exceptional disturbances. The simulation results for velocities are shown in Fig. 7, with the three curves corresponding to velocities in

https://doi.org/10.1017/aer.2022.47 Published online by Cambridge University Press

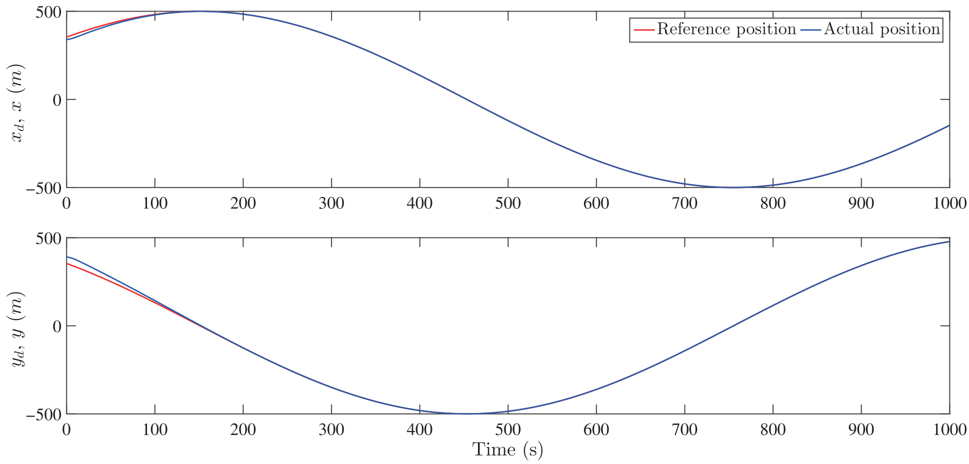

Figure 4. *Actual and reference positions.*

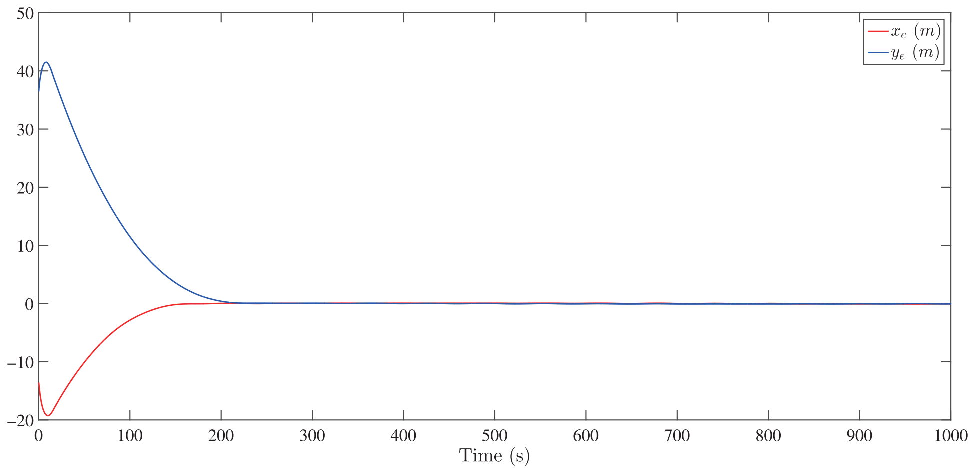

Figure 5. *Position errors x_e and y_e.*

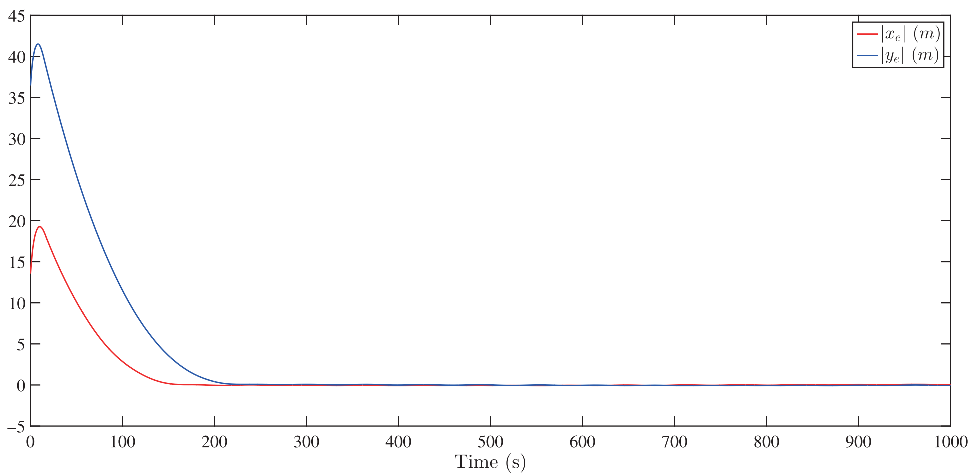

Figure 6. *Absolute values of the position errors x_e and y_e.*

https://doi.org/10.1017/aer.2022.47 Published online by Cambridge University Press

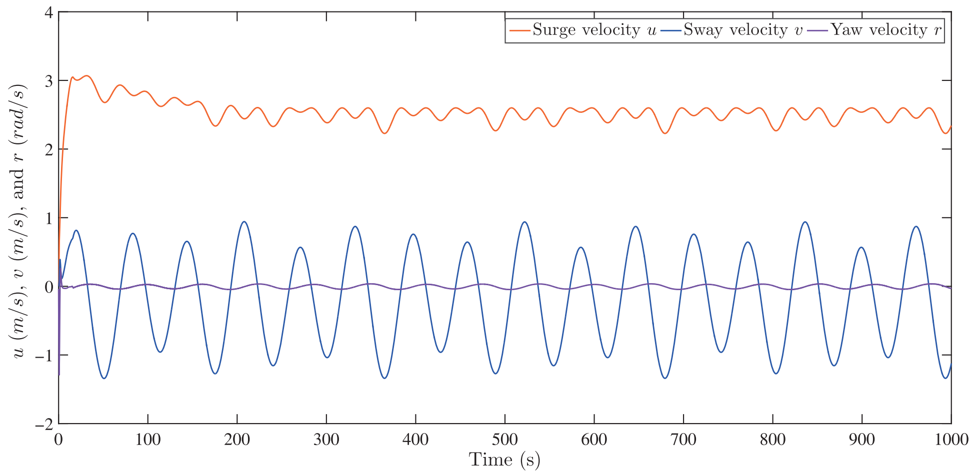

Figure 7. *Velocities in surge u, sway v, and yaw r.*

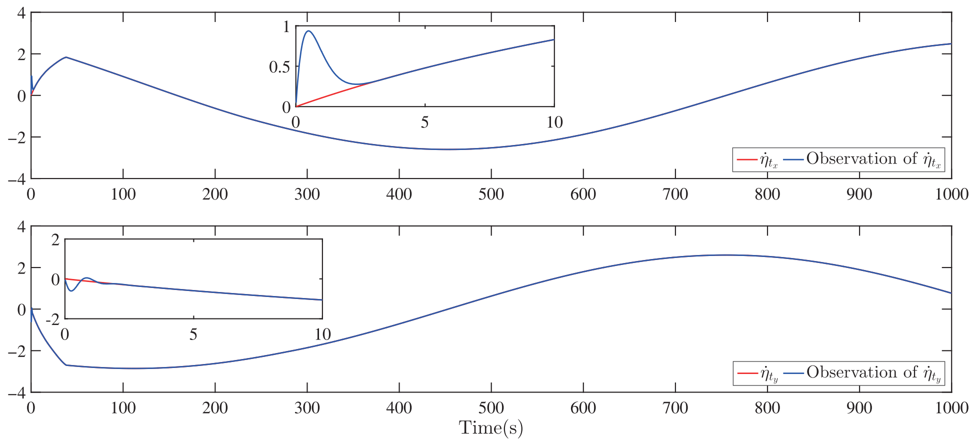

Figure 8. *Unmeasured state $\dot{\eta}_t$ (i.e., $\varkappa_2$) and its finite-time observation.*

the surge, sway and yaw, respectively, all of which are bounded for $\forall t \geq 0$ but do not enter a steady state. The reason is twofold. First, a circular path is allocated to track, yielding the desired velocities time-varying. Second, the persistent perturbations (9) consisting in the airship model (8) affect the system dynamics directly. Figures 8-9 plot the unmeasured velocity $\dot{\eta}_t$ (i.e., $\varkappa_2$), the lumped disturbances δ_{lu}, and their observed values, which show that the FTO (21) can supply the exact observations of $\dot{\eta}_t$ and δ_{lu} in a finite time. Figure 10 presents the necessary control action, from which we see that the surge force and yaw torque are continuous, and no control chattering exists. It should be noted that, compared with the actuating signal τ_r in the steady-state phase, it appears more aggressive in the initial stage. The reason is that the mass m_r is huge (12,176kg· m2), and the velocity is initialised to zero. As a result, a large control torque is required in the initial stage to accelerate the airship to the reference route. Nevertheless, it decreases quickly, as shown in Fig. 10. The trajectory tracking responses for different initial positions are depicted in Figs 11-13. It can be observed that the finite-time convergence is assured, and the requirement for tracking accuracy, featured in Equation (70), is also met. The above conclusions successfully affirm that a good tracking performance is achieved under our method.

https://doi.org/10.1017/aer.2022.47 Published online by Cambridge University Press

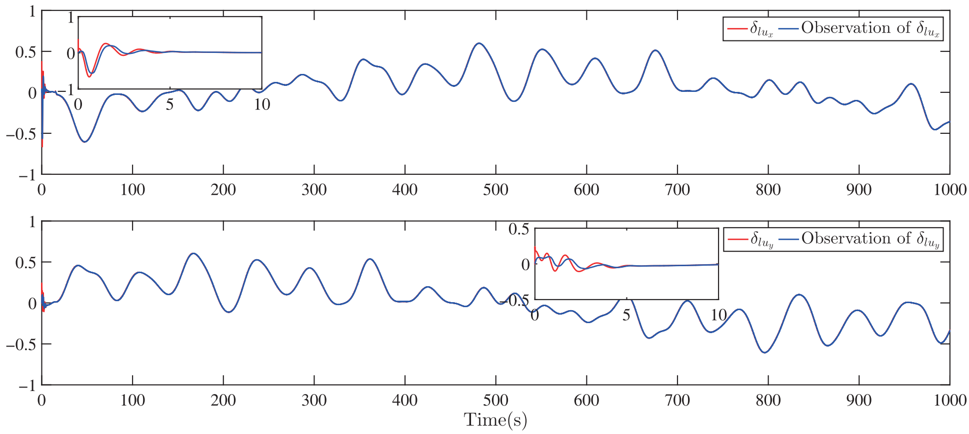

Figure 9. *Lumped disturbance δ_{lu_i} ($i = x, y$) and its finite-time observation.*

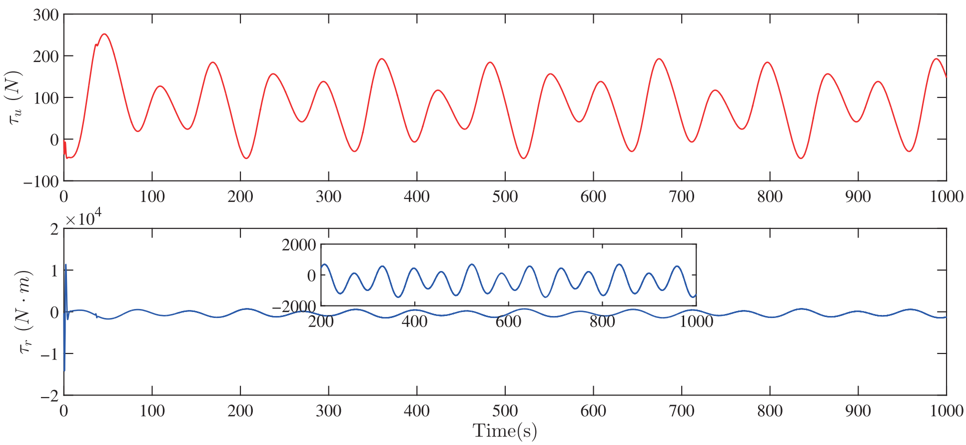

Figure 10. *Control signal τ.*

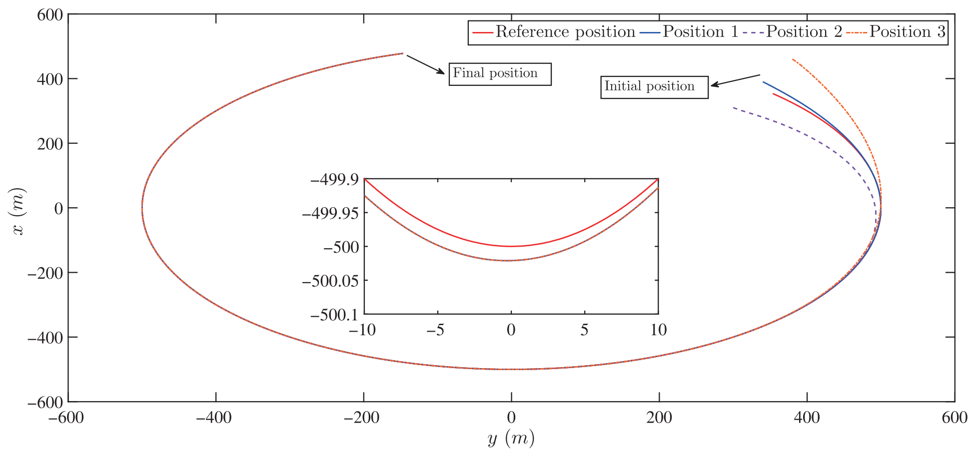

Figure 11. *Trajectories with different initial positions: [340m,390m] (position 1); [300m,310m] (position 2); [280m,460m] (position 3).*

https://doi.org/10.1017/aer.2022.47 Published online by Cambridge University Press

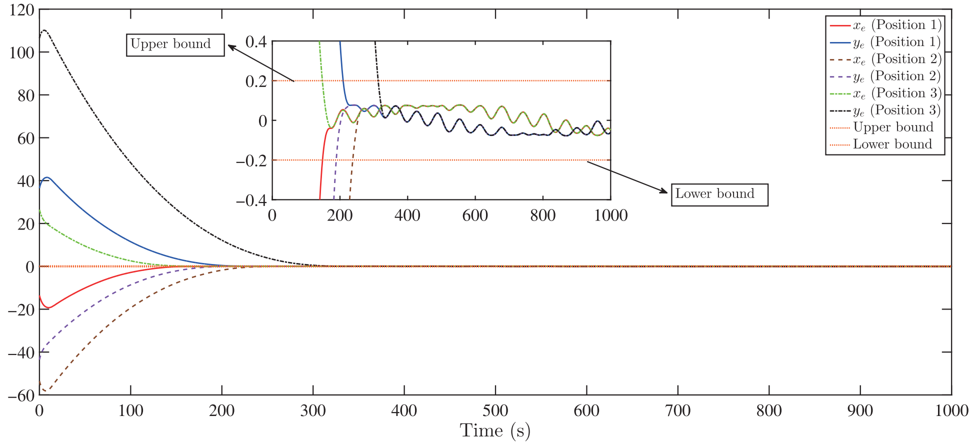

Figure 12. *Position errors x_e and y_e with different initial positions: [340m,390m] (position 1); [300m,310m] (position 2); [280m,460m] (position 3).*

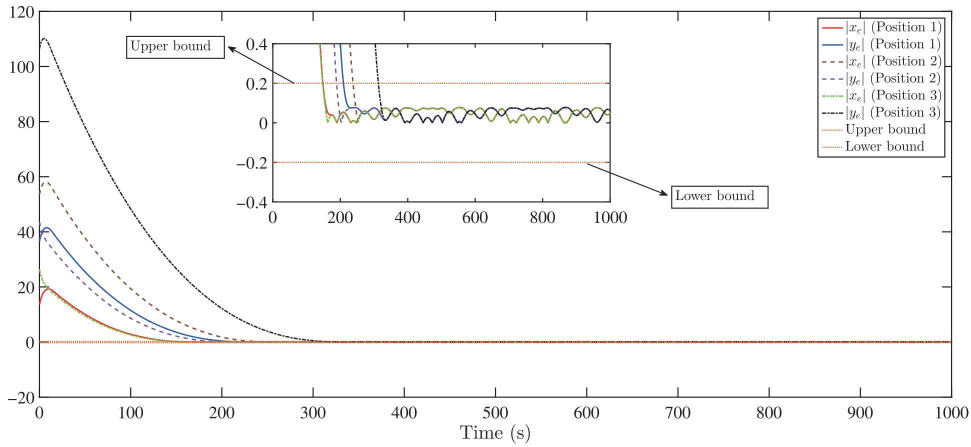

Figure 13. *Absolute values of the position errors x_e and y_e with different initial positions: [340m,390m] (position 1); [300m,310m] (position 2); [280m,460m] (position 3).*

Aimed at comparison, a standard command-filter backstepping (CFB) controller

$$\begin{cases} z_1 = \varkappa_1 - \eta_d, z_2 = \varkappa_2 - x_{2r} \\ \bar{z}_1 = z_1 - c_1, \bar{z}_2 = z_2 - c_2 \\ \dot{c}_1 = -k_1 c_1 + x_{2r} - x_{2r}^0, \dot{c}_2 = -k_2 c_2 + R(\psi) M_\epsilon \left(\tau - \tau^0\right) \\ x_{2r}^0 = a_1 - c_2, \tau^0 = a_2 \\ a_1 = -k_1 z_1 + \dot{\eta}_d, \tau^0 = a_2 = (R(\psi) M_\epsilon)^{-1} \left(-k_2 z_2 - \bar{z}_1 - F + \dot{x}_{2r}\right) \end{cases} \tag{73}$$

formulated by Han et al. [9] is introduced in this paper, where the control parameters $k_1 = k_2 = eye(3)$ are identical to those used by Han et al. [9]. The comparison results are illustrated in Figs 14-17, where FI control shorts for our method. Moreover, to further display the comparative simulations, we summarise the quantisation indexes in Table 2, where the integrated absolute error, IAE (defined as IAE $= \int_0^{T_{final}} |j_e(t)|\,dt, j = x, y$), the integrated time absolute error, ITAE (defined as ITAE $= \int_0^{T_{final}} t|j_e(t)|\,dt, j = x, y$), and the mean integrated absolute control, MIAC (defined as MIAC $= \frac{1}{T_{final}} \int_0^{T_{final}} |\tau_j(t)|\,dt, j = u, i$), devote to assess steady-state performance, transient performance, and control effort, respectively. As seen in Figs 14-17 and Table 2, it is clear that the tracking performance is not satisfactory under the CFB

https://doi.org/10.1017/aer.2022.47 Published online by Cambridge University Press

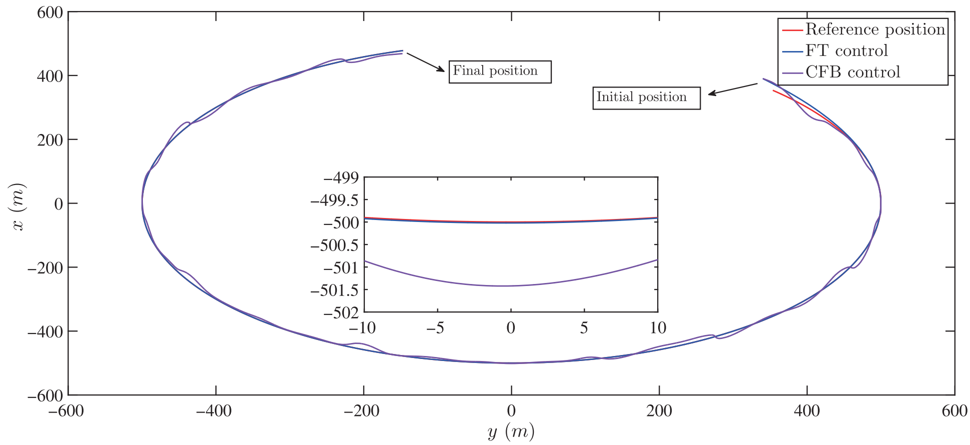

Figure 14. *Trajectories based on FT control and CFB control.*

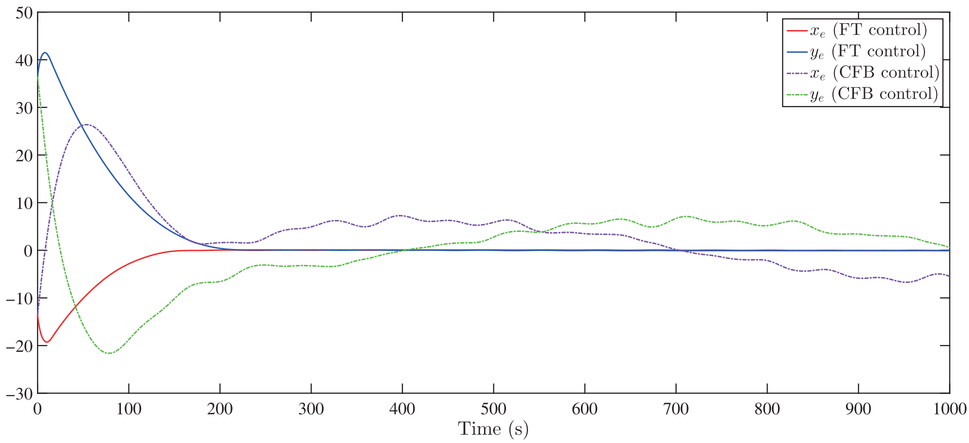

Figure 15. *Position errors x_e and y_e based on FT control and CFB control.*

Table 2. *Performance indices comparisons*

Index	Item	FI control	CFB control
2IAE	x_e	756.4	5.9×10^3
	y_e	1.8×10^3	5.8×10^3
ITAE	x_e	5.5×10^4	2.2×10^6
	y_e	1.4×10^5	2.1×10^6
MIAC	τ_u	87.4	93.9
	τ_r	730.1	1.5×10^3

controller and large position errors emerge in the steady state, although the CFB controller ensures the boundedness of position errors. Particularly, the robustness of the CFB controller cannot be warranted in default of a compensation mechanism versus modeling imprecisions and disturbances, as demonstrated in Figs 15-16. In addition, compared to our method, the CFB controller has the biggest IAE, ITAE and MIAC values. This indicates that our method can offer a better tracking quality with less control energy consumption.

https://doi.org/10.1017/aer.2022.47 Published online by Cambridge University Press

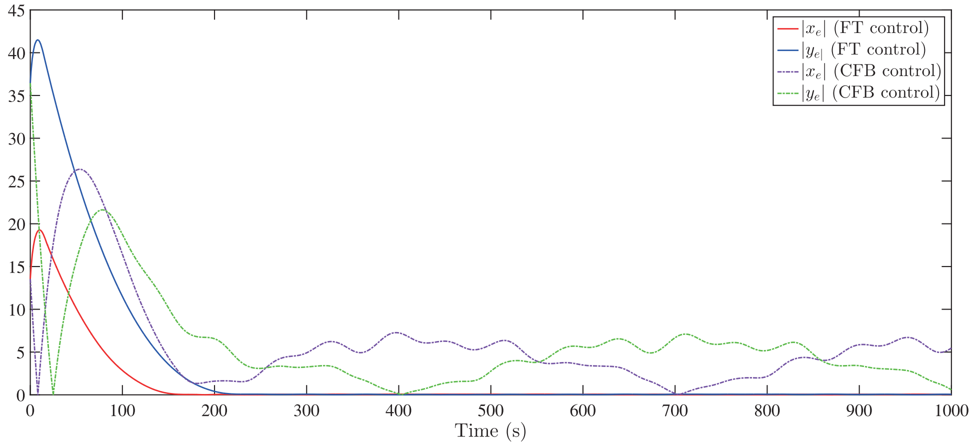

Figure 16. *Absolute values of the position errors x_e and y_e based on FT control and CFB control.*

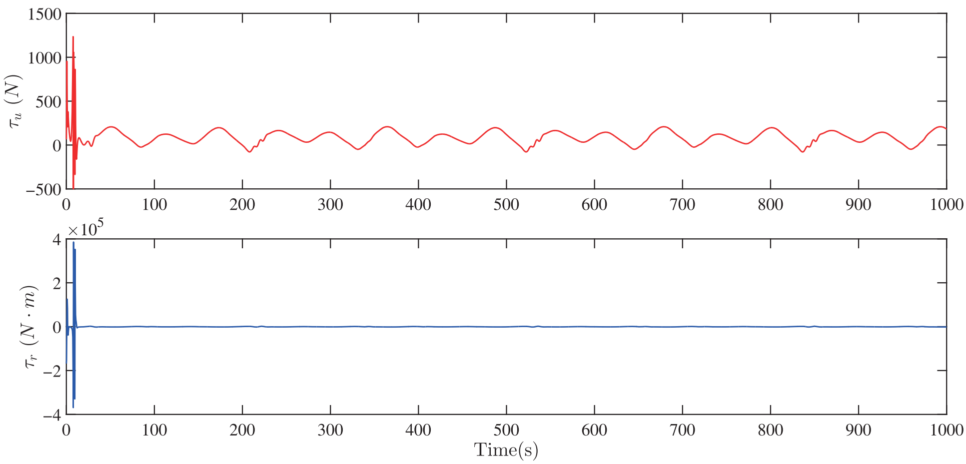

Figure 17. *Control signal τ based on CFB control.*

5.3 Discussion

This paper studies the horizontal trajectory tracking control problem of airships. The system model is built upon Assumption 1, which is widely made in the related literature [3, 6, 10, 17, 18, 22, 23]. Assumption 2 is introduced to give some characterisation of unmodeled dynamics and external disturbances, as the exact model of airships is not always attainable in reality, and the persistent wind field directly affects the motion of airships and thus cannot be neglected in the design of a tracker. From Equation (8), we easily find that the airship, flying in the horizontal plane, is a typical underactuated system. To this end, we start our research with a coordinate transformation (11). After a series of reasoning shown in Equations (12)–(17), a fully actuated EL model (18) is obtained. From Figs 3-6, we see that the coordinate transformation (11) does solve the underactuated problem. We then present an FTO (21) that requires Assumption 4 to realise the velocity-free control and the dynamical compensation. The main property of the FTO (21) is given in Theorem 1, and the reasonability of Assumption 4 is given in Remark 5. Figures 8-9 demonstrate the effectiveness of the FTO (21). Note that in the current literature on API technique [30–35], certain control parameters are restricted to ratios of positive odd integers. Based on Lemma 4, we relax this restriction. The selection for α shows this advantage. Finally, in the light of Lemmas 1–5, we propose an API-based finite trajectory tracking control algorithm for

https://doi.org/10.1017/aer.2022.47 Published online by Cambridge University Press

underactuated airships without command filters or dynamic surfaces. Figures 11–12 illustrate the finite-time convergence of position errors to a preassigned residual set, validating the theoretical predictions in Remark 4 and Theorem 2.

6.0 Conclusion

This brief presented a novel finite-time velocity-free trajectory tracking control algorithm for an underactuated airship under the condition of modeling imperfections and environmental disturbances. First, a coordinate transformation was conducted to address the underactuated problem, which make the presented approach can be extended easily to a wide range of second-order mechanical systems. Second, an FTO was built to form a output-feedback control structure with disturbance estimation and attenuation ability. Finally, we blended the backstepping technique and API method into a Lyapunov design, which successfully guaranteed the finite-time convergence of the position errors x_e and y_e into a preassigned residual set around zero. The control design did not cover any analytically formidable calculation, filters, or self-tuning mechanisms (e.g. FLSs or NNs), leading to a structurally simple control attribute. Our future work will focus on extending this approach to a stratospheric airship with actuator faults.

Acknowledgment. This work was supported in part by the National Natural Science Foundation of China (Nos. 51205253 and 51906141).

Conflicts interest. There is no conflict of interest.

References

[1] Dancila, R.I. and Botez, R.M. New flight trajectory optimisation method using genetic algorithms, *Aeronaut. J.*, 2021, **125**, (1286), pp 618–671.
[2] Khoury, G.A. *Airship Technology*, vol. **10**, Cambridge University Press, 2012, Cambridge, UK.
[3] Yang, X., Yang, X. and Deng, X. Horizontal trajectory control of stratospheric airships in wind field using q-learning algorithm, *Aerospace Sci. Technol.*, 2020, **106**, p 106100.
[4] Manikandan, M. and Pant, R.S. A comparative study of conventional and tri-lobed stratospheric airships, *Aeronaut. J.*, 2021, **125**, (1290), pp 1434–1466.
[5] Agrawal, S., Gobiha, D. and Sinha, N.K. Nonlinear parameter estimation of airship using modular neural network, *Aeronaut. J.*, 2020, **124**, (1273), pp 409–428.
[6] Zheng, Z., Guan, Z., Ma, Y. and Zhu, B. Constrained path-following control for an airship with uncertainties, *Eng. Appl. Artif. Intell.*, 2019, **85**, pp 295–306.
[7] Chen, L., Gao, Q., Deng, Y. and Liu, J. Moving-mass-based station keeping of stratospheric airships, *Aeronaut. J.*, 2021, **125**, (1289), pp 1231–1244.
[8] Yang, Y., Xu, X., Zhang, B., Zheng, W. and Wang, Y. Bionic design for the aerodynamic shape of a stratospheric airship, *Aerospace Sci. Technol.*, 2020, **98**, p 105664.
[9] Han, D., Wang, X., Chen, L. and Duan, D. Command-filtered backstepping control for a multi-vectored thrust stratospheric airship, *Trans. Inst. Meas. Control*, 2016, **38**, (1), pp 93–104.
[10] Wu, Y., Wang, Q., Duan, D., Xie, W. and Wei, Y. Neuroadaptive output-feedback trajectory tracking control for a stratospheric airship with prescribed performance, *Aeronaut. J.*, 2020, **124**, (1280), pp 1568–1591.
[11] Yang, Y. A time-specified nonsingular terminal sliding mode control approach for trajectory tracking of robotic airships, *Nonlinear Dyn.*, 2018, **92**, (3), pp 1359–1367.
[12] Meng, F., Zhao, L. and Yu, J. Backstepping based adaptive finite-time tracking control of manipulator systems with uncertain parameters and unknown backlash, *J. Franklin Inst.*, 2020, **357**, (16), pp 11281–11297.
[13] Sabiha, A.D., Kamel, M.A., Said, E. and Hussein, W.M. Ros-based trajectory tracking control for autonomous tracked vehicle using optimized backstepping and sliding mode control, *Rob. Auto. Syst.*, 2022, **152**, p 104058.
[14] Xiao, C., Han, D., Wang, Y., Zhou, P. and Duan, D. Fault-tolerant tracking control for a multi-vectored thrust ellipsoidal airship using adaptive integral sliding mode approach, *Proc. Inst. Mech. Eng. Part G J. Aerospace Eng.*, 2018, **232**, (10), pp 1911–1924.
[15] Yang, Y. Positioning control for stratospheric satellites subject to dynamics uncertainty and input constraints, *Aerospace Sci. Technol.*, 2019, **86**, pp 534–541.
[16] Sun, K., Liu, L., Qiu, J. and Feng, G. Fuzzy adaptive finite-time fault-tolerant control for strict-feedback nonlinear systems, *IEEE Trans. Fuzzy Syst.*, 2020, **29**, (4), pp 786–796.
[17] Zheng, Z. and Xie, L. Finite-time path following control for a stratospheric airship with input saturation and error constraint, *Int. J. Control*, 2019, **92**, (2), pp 368–393.
[18] Yan, Z., Weidong, Q., Yugeng, X. and Zili, C. Stabilization and trajectory tracking of autonomous airship's planar motion, *J. Syst. Eng. Electron.*, 2008, **19**, (5), pp 974–981.

https://doi.org/10.1017/aer.2022.47 Published online by Cambridge University Press

[19] Yamada, M., Adachi, H. and Funahashi, Y. Robust control of an uncertain underactuated airship with asymptotic rejection against wind disturbance, 2010 *IEEE International Conference on Control Applications, IEEE*, 2010, pp 1844–1849.
[20] Dai, S.-L., He, S. and Lin, H. Transverse function control with prescribed performance guarantees for underactuated marine surface vehicles, *Int. J. Robust Nonlinear Control*, 2019, **29**, (5), pp 1577–1596.
[21] Jia, Z., Hu, Z. and Zhang, W. Adaptive output-feedback control with prescribed performance for trajectory tracking of underactuated surface vessels, *ISA Trans.*, 2019, **95**, pp 18–26.
[22] Yang, Y., Wu, J. and Zheng, W. Station-keeping control for a stratospheric airship platform via fuzzy adaptive backstepping approach, *Adv. Space Res.*, 2013, **51**, (7), pp 1157–1167.
[23] Azinheira, J.R., Moutinho, A. and De Paiva, E.C. Airship hover stabilization using a backstepping control approach, *J. Guidance Control Dyn.*, 2006, **29**, (4), pp 903–914.
[24] Anjum, Z. and Guo, Y. Finite time fractional-order adaptive backstepping fault tolerant control of robotic manipulator, *Int. J. Control Autom. Syst.*, 2021, **19**, (1), pp 301–310.
[25] Ovcharov, A., Vedyakov, A., Kazak, S. and Pyrkin, A. Overparameterized model parameter recovering with finite-time convergence, *Int. J. Adapt. Control Signal Process.*, 2022.
[26] Rocha, E., Castaños, F. and Moreno, J.A. Robust finite-time stabilisation of an arbitrary-order nonholonomic system in chained form, *Automatica*, 2022, **135**, p 109956.
[27] Zhang, J., Tong, S.-C. and Li, Y.-M. Adaptive fuzzy finite-time output-feedback fault-tolerant control of nonstrict-feedback systems against actuator faults, *IEEE Trans. Syst. Man Cybern. Syst.*, 2020, **52**, pp 1276–1287.
[28] Huang, Y., Wang, J., Wang, F. and He, B. Event-triggered adaptive finite-time tracking control for full state constraints nonlinear systems with parameter uncertainties and given transient performance, *ISA Trans.*, 2021, **108**, pp 131–143.
[29] Shen, D., Tang, L., Hu, Q., Guo, C., Li, X. and Zhang, J. Space manipulator trajectory tracking based on recursive decentralized finite-time control, *Aerospace Sci. Technol.*, 2020, **102**, p 105870.
[30] Du, H., Zhang, J., Wu, D., Zhu, W., Li, H. and Chu, Z. Fixed-time attitude stabilization for a rigid spacecraft, *ISA Trans.*, 2020, **98**, pp 263–270.
[31] Sun, H., Hou, L., Zong, G. and Yu, X. Fixed-time attitude tracking control for spacecraft with input quantization, *IEEE Trans. Aerospace Electron. Syst.*, 2018, **55**, (1), pp 124–134.
[32] Zhang, Z. and Wu, Y. Fixed-time regulation control of uncertain nonholonomic systems and its applications, *Int. J. Control*, 2017, **90**, (7), pp 1327–1344.
[33] Yang, Y., Hua, C., Li, J. and Guan, X. Robust adaptive uniform exact tracking control for uncertain euler–lagrange system, *Int. J. Control*, 2017, **90**, (12), pp 2711–2720.
[34] Zheng, Z., Feroskhan, M. and Sun, L. Adaptive fixed-time trajectory tracking control of a stratospheric airship, *ISA Trans.*, 2018, **76**, pp 134–144.
[35] Fu, M., Wang, T. and Wang, C. Fixed-time trajectory tracking control of a full state constrained marine surface vehicle with model uncertainties and external disturbances, *Int. J. Control Autom. Syst.*, 2019, **17**, (6), pp 1331–1345.
[36] Yang, Y., Wu, J. and Zheng, W. Design, modeling and control for a stratospheric telecommunication platform, *Acta Astronautica*, 2012, **80**, pp 181–189.
[37] Zhou, W., Zhou, P., Wang, Y., Wang, N. and Duan, D. Station-keeping control of an underactuated stratospheric airship, *Int. J. Fuzzy Syst.*, 2019, **21**, (3), pp 715–732.
[38] Yang, Y., Wu, J. and Zheng, W. Trajectory tracking for an autonomous airship using fuzzy adaptive sliding mode control, *J. Zhejiang Univ. Sci. C*, 2012, **13**, (7), pp 534–543.
[39] Funk, P., Lutz, T. and Wagner, S. Experimental investigations on hull-fin interferences of the lotte airship, *Aerospace Sci. Technol.*, 2003, **7**, (8), pp 603–610.
[40] Zhang, J., Yu, S. and Yan, Y. Fixed-time output feedback trajectory tracking control of marine surface vessels subject to unknown external disturbances and uncertainties, *ISA Trans.*, 2019, **93**, pp 145–155.
[41] Zhang, J., Yu, S. and Yan, Y. Fixed-time velocity-free sliding mode tracking control for marine surface vessels with uncertainties and unknown actuator faults, *Ocean Eng.*, 2020, **201**, p 107107.
[42] Zhang, L., Wei, C., Wu, R. and Cui, N. Fixed-time extended state observer based non-singular fast terminal sliding mode control for a vtvl reusable launch vehicle, *Aerospace Sci. Technol.*, 2018, **82**, pp 70–79.
[43] Basin, M., Yu, P. and Shtessel, Y. Finite-and fixed-time differentiators utilising hosm techniques, *IET Control Theory Appl.*, 2017, **11**, (8), pp 1144–1152.
[44] Cruz-Zavala, E., Moreno, J.A. and Fridman, L.M. Uniform robust exact differentiator, *IEEE Trans. Autom. Control*, 2011, **56**, (11), pp 2727–2733.

Cite this article: Wu Y., Wang Q. and Duan D. (2023). Finite-time velocity-free trajectory tracking control for a stratospheric airship with preassigned accuracy. *The Aeronautical Journal*, **127**, 139–162. https://doi.org/10.1017/aer.2022.47